



HAL
open science

Plume mantle source heterogeneity through time: Insights from the Duarte Complex, Hispaniola, northeastern Caribbean

Javier Escuder-Viruete, Andrés Pérez-Estaún, Fernando Contreras, Marc Joubert, Dominique Weis, Thomas Ullrich, Piera Spadea

► To cite this version:

Javier Escuder-Viruete, Andrés Pérez-Estaún, Fernando Contreras, Marc Joubert, Dominique Weis, et al.. Plume mantle source heterogeneity through time: Insights from the Duarte Complex, Hispaniola, northeastern Caribbean. *Journal of Geophysical Research*, 2007, 112 (B4), 10.1029/2006jb004323 . hal-03645465

HAL Id: hal-03645465

<https://brgm.hal.science/hal-03645465>

Submitted on 19 Apr 2022

HAL is a multi-disciplinary open access archive for the deposit and dissemination of scientific research documents, whether they are published or not. The documents may come from teaching and research institutions in France or abroad, or from public or private research centers.

L'archive ouverte pluridisciplinaire **HAL**, est destinée au dépôt et à la diffusion de documents scientifiques de niveau recherche, publiés ou non, émanant des établissements d'enseignement et de recherche français ou étrangers, des laboratoires publics ou privés.

Plume mantle source heterogeneity through time: Insights from the Duarte Complex, Hispaniola, northeastern Caribbean

Javier Escuder-Virue, ¹ Andrés Pérez-Estaún, ² Fernando Contreras, ³ Marc Joubert, ⁴ Dominique Weis, ⁵ Thomas D. Ullrich, ⁵ and Piera Spadea ^{6,7}

Received 2 February 2006; revised 2 November 2006; accepted 27 November 2006; published 11 April 2007.

[1] Located in the Cordillera Central of Hispaniola, the Duarte Complex offers an opportunity to study an on-land fragment of the Caribbean-Colombian oceanic plateau. Geochemical, Sr-Nd isotope, and ⁴⁰Ar-³⁹Ar radiometric age data combined with detailed mapping have shown that the Duarte Complex includes two lithostratigraphic units, composed of four geochemical groups of metavolcanic rocks: Group Ia, low-Ti high-Mg basalts, and group Ib, high-Ti picrites and primitive high-Mg basalts, occur interlayered in the lowermost levels of the lower unit; group II, light rare earth element (LREE)-enriched picrites, ferropicrites and high-Mg basalts, forms the main lava sequence of the lower unit; and group III, LREE-enriched Fe-Ti basalts, is present exclusively in the upper unit. Nd isotope and incompatible trace element patterns are diverse in the Duarte Complex metavolcanics and are consistent with mantle sources related to a heterogeneous plume. Mantle melt modeling suggests that an early, extensive melting (10–20%) of shallow mantle resulted in the formation of relatively depleted group I and II magmas, whereas the late, more enriched group III magmas were the product of deeper, low-degree (<3%) melting of a heterogeneous plume. Therefore plume mantle sources were more enriched and deeper through time. Foliated amphibolites of the Duarte Complex yield ⁴⁰Ar-³⁹Ar hornblende plateau ages of 93.9 ± 1.4 and 95.8 ± 1.9 Ma (Cenomanian, 99.6–93.5 Ma) that demonstrate an older age of the protholiths, probably Albian (>96 Ma). Hence an Early Cretaceous phase of the Caribbean-Colombian oceanic plateau construction is recorded in Hispaniola.

Citation: Escuder-Virue, J., A. Pérez-Estaún, F. Contreras, M. Joubert, D. Weis, T. D. Ullrich, and P. Spadea (2007), Plume mantle source heterogeneity through time: Insights from the Duarte Complex, Hispaniola, northeastern Caribbean, *J. Geophys. Res.*, 112, B04203, doi:10.1029/2006JB004323.

1. Introduction

[2] Mantle plumes provide the most convincing explanation of voluminous Phanerozoic volcanism that generated large igneous provinces (LIPs), both on intraoceanic ridge and intraplate [Coffin and Eldholm, 1994]. LIPs formation can be closely associated space and in time with supercontinent breakup, juvenile crust production, and environmental stress responsible for global mass extinction events [Saunders et al., 1996; Arndt, 1999; Frey et al., 2003; Ernst et al., 2005]. The geochemical characteristics of plume magmatic products (komatiites, picrites and high-Mg basalts)

suggest that the mantle sources were deep or subasthenosphere, and that the magmas were generated by dynamic melting at pressures of 3–4 GPa in an ascending plume [Arndt et al., 1997; Kerr et al., 2002; Herzberg and O'Hara, 2002; Kerr, 2005]. Melting processes in the mantle at these high pressures are consistent with low-velocity anomalies obtained by geophysical tomographic techniques, which have yielded, for instance, high-resolution images of Atlantic mantle plumes, as found in Iceland, Azores and Eifel, down to 400 km depth [Pilidou et al., 2005].

[3] To account for the range of radiogenic isotope and incompatible element ratios found in plume-related oceanic basalts, distinct (two or more) mantle sources, both depleted and enriched relative to bulk earth have been considered [Dupré and Echeverría, 1984; Arndt et al., 1997; Kerr et al., 1996, 1997a; Révillon et al., 2002]. Recent models of the source regions and melting depths of the chemically diverse magma types are based on a heterogeneous mantle plume source or favor mixing of melts derived from the plume and nearby mid-ocean ridge basalt (MORB)-depleted mantle [Kerr et al., 1995, 2002; Fitton et al., 1997, 2003; Weis and Frey, 2002]. To account for the diversity of melts from a heterogeneous mantle plume, the enriched magma

¹Instituto Geológico y Minero de España, Madrid, Spain.

²Institut de Ciències de la Terra Jaume Almera, Consejo Superior de Investigaciones Científicas, Barcelona, Spain.

³Informes y Proyectos, S.A., Madrid, Spain.

⁴Bureau de Recherches Géologiques et Minières, Orléans, France.

⁵Pacific Centre for Isotopic and Geochemical Research, University of British Columbia, Vancouver, Canada.

⁶Dipartimento di Georisorse e Territorio, Università degli Studi di Udine, Udine, Italy.

⁷Deceased August 2006.

types are considered to be the products of deep, small degree melting of a plume composed of a refractory matrix with fusible, enriched blobs, whereas the more depleted magmas are related to shallower, more extensive melting. Thus a pervasive heterogeneous mantle plume source can explain the geochemical diversity displayed by the oceanic plateau lavas. According to these models the initial deep (>150 km), low-degree melting of relatively depleted mantle generates enriched picritic magmas. These high-P, low-volume, melts mostly crystallize in the cooler top of the plume, near the base of the lithosphere. Occasionally they may erupt, as shown by the enriched picrites from Cretaceous oceanic plateau sequences of Gorgona, Colombia [Kerr, 2005], Colombian Andes [Kerr et al., 2002], Costa Rica [Hauff et al., 2000b] and of the Duarte Complex of Hispaniola [Lapierre et al., 1997, 2000].

[4] The Duarte Complex is included in the Caribbean-Colombian oceanic plateau (CCOP [Kerr et al., 1997b]) and offers us an opportunity to study an on-land crustal section of an oceanic plateau. In this paper, we present new lithostratigraphic, ^{40}Ar - ^{39}Ar ages, geochemical and Sr-Nd isotopic data on the volcanic rocks and their metamorphic equivalents of the Duarte Complex, recently investigated in detail during the geological mapping of Hispaniola. The aims of this work are to determine whether the Duarte Complex igneous rocks are part of a multiphase Cretaceous CCOP; to constrain the temporal extent of this plume-related volcanism; and to document the heterogeneous nature of the mantle plume source involved in its petrogenesis through time.

2. Geodynamic Setting

2.1. Caribbean-Colombian Oceanic Plateau

[5] The CCOP is a part of a large Cretaceous oceanic plateau derived from the Pacific plate and now exposed in and around the Caribbean plate, and in accreted terranes from northwestern South America (see reviews of Donnelly et al. [1990], Kerr et al. [1997b], and Sinton et al. [1998]). Onland exposed sequences of the CCOP outcrop in Cuba, Jamaica, Hispaniola, coastal bordelands of Venezuela, Curaçao and Aruba islands, the Pacific coast of Central America and western Colombia. The submerged portion of the plateau in the Caribbean Sea was sampled by drilling during Deep Sea Drilling Project (DSDP) Leg 15 and Ocean Drilling Program (ODP) Leg 163 [Sinton et al., 2000]. It is generally accepted that the Caribbean plate was generated during the Cretaceous in the eastern Pacific as a LIP [Duncan and Hargreaves, 1984; Kerr et al., 1997b]. Eastward movement of the Farallon plate in the Late Cretaceous-Early Tertiary forced the motion of the northern half of the CCOP into the ocean basin, which had been opening between North and South America since Jurassic [Mann, 1999; Pindell et al., 2005, 2006]. Using a fixed hot spot reference frame, Duncan and Hargreaves [1984] suggested that the magmas of the CCOP produced by partial melting within the initial “plume head” of the Galápagos hot spot. However, Meschede [1998] argues against a Galápagos origin for the CCOP and Kerr and Tarney [2005] propose that the CCOP results from the accretion of two separated Late Cretaceous oceanic plateaus, related to two independent hot spots.

[6] The CCOP consists of volcanic rocks erupted during two, possibly three, phases of broadly different age. The ages compiled by Kerr et al. [1997b, 2002] include a 124–112 Ma (Aptian) phase [Lapierre et al., 2000], a 94–83 Ma phase (the most voluminous) and a 78–72 Ma phase. These phases have been also recognized by Hoernle et al. [2004] in Costa Rica and in other Cretaceous oceanic plateaus from the western Pacific [Neal et al., 1997; Ernst et al., 2005], where plume magmatism occurred for 50 Ma or more at variable eruptive rates. The youngest CCOP rocks are found in the Dominican Republic (69 Ma) and the Quepos Peninsula of Costa Rica (63 Ma) [Sinton et al., 1998]. Though the CCOP comprises a wide diversity of basaltic magma compositions, the vast majority of the lavas possess depleted signatures with ϵ_{Nd} ranging from +8.5 to +6.0 and flat to slightly LREE-enriched chondrite normalized patterns [Kerr et al., 1996, 1997a; Sinton et al., 1998; Hauff et al., 2000a, 2000b; Lapierre et al., 2000]. Picrites have been reported among the volcanic sequences in the CCOP, which are geochemically similar to the komatiitic lavas from Gorgona Island [Kerr et al., 1996]. Relatively immobile high field strength element (HFSE) ratios and Pb-Nd-Hf isotopic systematics in the CCOP plume-related basalts indicate the presence of end-member HIMU and enriched mantle components (EM), which may result from recycling subduction-related material to the deep mantle and later upwelling in a rising mantle plume [Hauff et al., 2000a; Révillon et al., 2000; Lapierre et al., 2000].

2.2. Occurrences of the Caribbean-Colombian Oceanic Plateau in Hispaniola

[7] In Hispaniola, fragments of plume-derived, obducted/accreted oceanic plateaus include the Dumisseau Formation in southwestern Haiti [Sen et al., 1988], the Siete Cabezas Formation [Donnelly et al., 1990; Sinton et al., 1998], and the Duarte Complex in Central Cordillera (Figure 1) [Lewis et al., 1983, 2002; Draper and Lewis, 1989, 1991; Lewis and Jiménez, 1991; Lapierre et al., 1997, 2000]. The Dumisseau Formation consists of pillowed and massive basalts and minor picrites interlayered with pelagic limestones, volcanogenic and biogenic turbidites, cherts, and siltstones. Fossil ages of the sediments are Early Cretaceous to Santonian for the lower basalts, and Late Campanian for the upper basalts. Sinton et al. [1998] obtained ^{40}Ar - ^{39}Ar ages between 88.7 ± 1.5 and 92.0 ± 4.8 for the lower basalts. However, the upper basalts of the Dumisseau Formation should be younger, given the Late Campanian fossil age of the sediments and the 75.0 ± 1.5 Ma K-Ar age provided by a late stage sill intruding the upper sequence [Sen et al., 1988]. The Dumisseau Formation is overlain by late Campanian to Maastrichtian limestones. The Siete Cabezas Formation is composed of mostly massive and pillowed, aphyric basalts, with minor pyroclastic breccias, vitric tuffs and cherts, intruded by dolerite dikes [de Lepinay, 1987]. Radiolaria from these sediments yield middle Campanian to Maastrichtian ages [Montgomery and Pessagno, 1999]. Sinton et al. [1998] obtained consistent ^{40}Ar - ^{39}Ar ages for whole rock (69.0 ± 0.7 Ma) and plagioclase (68.5 ± 0.5 Ma). These ages and the geochemical characteristics of the lavas (tholeiitic basalts with flat REE patterns) have permitted Sinton et al. [1998] and Lewis et al. [2002] to attribute the Siete Cabezas Formation to the CCOP.

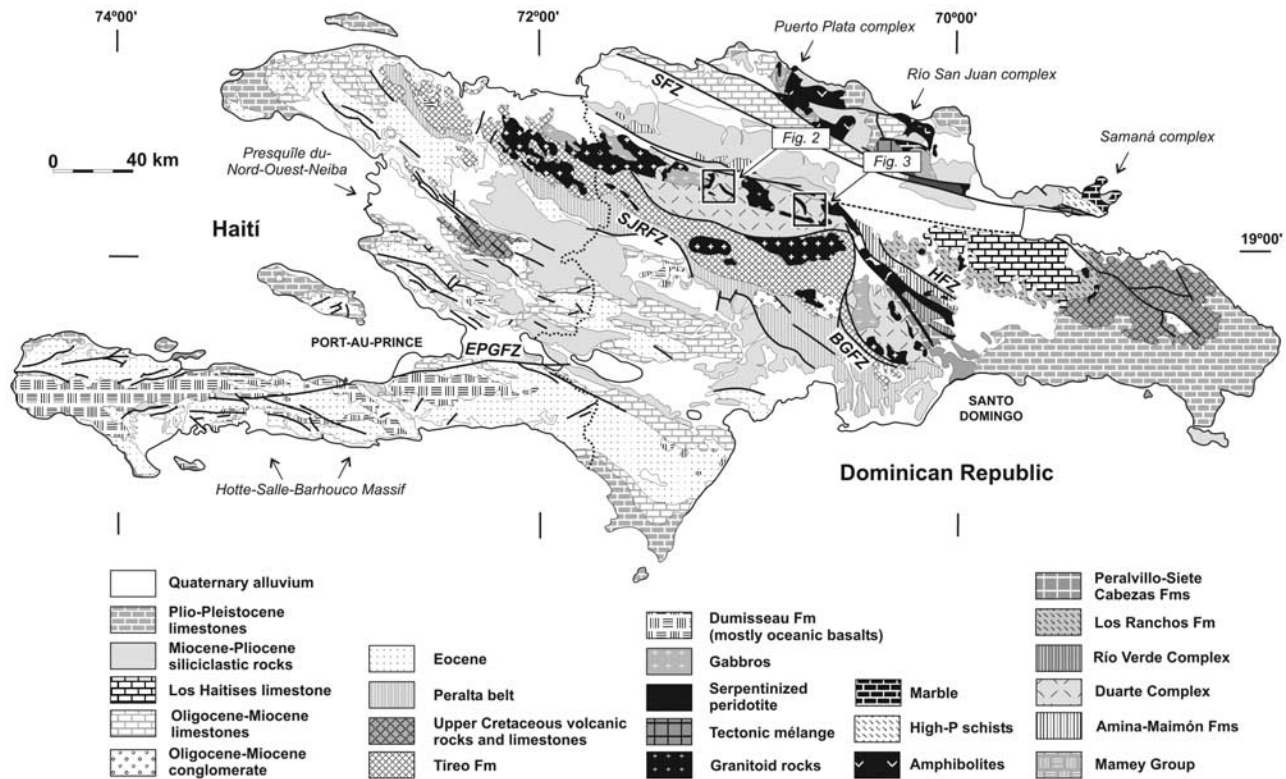


Figure 1. Geological map of Hispaniola Island (modified from *Draper and Lewis* [1991]). SFZ, Septentrional fault zone; HFZ, Hispaniola fault zone; BGFZ, Bonaio-La Guácara fault zone; SJRFZ, San Juan-Restauración fault zone; EPGFZ, Enriquillo-Plantain Garden fault zone. Boxes show maps of the Duarte Complex in Figures 2 and 3.

[8] The Duarte Complex comprises a ~3-km-thick sequence of heterogeneously deformed and metamorphosed mafic to ultramafic igneous rocks, intruded by arc-related batholiths [*Palmer*, 1979]. The complex includes olivine-clinopyroxene pyritic picrites and high-Mg basalts chemically related to plume-generated magmas [*Draper and Lewis*, 1991; *Lewis and Jiménez*, 1991]. *Draper and Lewis* and *Lewis and Jiménez* suggested that the Duarte Complex represents Late Jurassic-Early Cretaceous ocean islands or a seamount chain. *Lapierre et al.* [1997] described in detail the petrology and geochemistry of representative picrites, ultramafic cumulates and dolerites from the complex, and proposed an enriched mantle origin for these rocks, as shown by their enriched MORB (EMORB) affinity and Sr-Nd isotopic features similar to those of CCOP lavas. According to *Lapierre et al.*, the Duarte Complex represents the remnants of the proto-Caribbean plateau generated around 150 Ma by a Galápagos-type hot spot. In a later paper, *Lapierre et al.* [1999] report ^{40}Ar - ^{39}Ar cooling ages of 86.1 ± 1.3 Ma for amphiboles from metapicrites, and 86.7 ± 1.6 Ma for amphibolites that suggest a younger age of the Duarte Complex, contemporaneous with that of the Late Cretaceous basalts drilled during the DSDP Leg 15 *Sinton et al.* [2000]. In a recent paper, *Lewis et al.* [1999] argue that the 87–86 Ma radiometric ages obtained by *Lapierre et al.* [1999] on metamorphic amphiboles, are the result of thermal effects associated with orogenic metamorphism and/or intrusion of granitoids.

2.3. Geologic Setting of the Central Cordillera of Hispaniola

[9] Located in the northern margin of the Caribbean plate, the tectonic collage of Hispaniola island (Figure 1) results from the WSW to SW directed oblique convergence of the continental margin of the North American plate with the Cretaceous Caribbean island arc system, which began in Eocene to early Miocene times and continues today (see review by *Mann* [1999]). The arc-related rocks are regionally overlain by Upper Eocene to Holocene siliciclastic and carbonate sedimentary rocks that postdate island arc activity, and record the oblique arc-continent collision in the north, as well as the active subduction in the southern Hispaniola margin. Central Hispaniola is a composite of oceanic derived units bound by the left-lateral strike-slip Hispaniola and Bonaio-Guácara fault zones (Figure 1). Accreted units mainly include the Late Jurassic Loma La Monja volcanoplutonic assemblage that is remnant of the crust and mantle of the proto-Caribbean [*Escuder-Viruete et al.*, 2004]; the Lower Cretaceous oceanic plateau of the Duarte Complex; and the Upper Cretaceous arc-related rocks of the Tiroe Formation [*Lewis et al.*, 2002]. Central Hispaniola underwent deformation by regional subvertical shearing forming folds, thrust, and left-lateral shear zones and faults during the Coniacian-Santonian (90–84 Ma) to the Middle Campanian (77–74 Ma), and was accompanied by the intrusion of synkinematic to late kinematic gabbro-tonalitic batholiths [*Escuder-Viruete et al.*, 2006]. Sedimentary basins filled

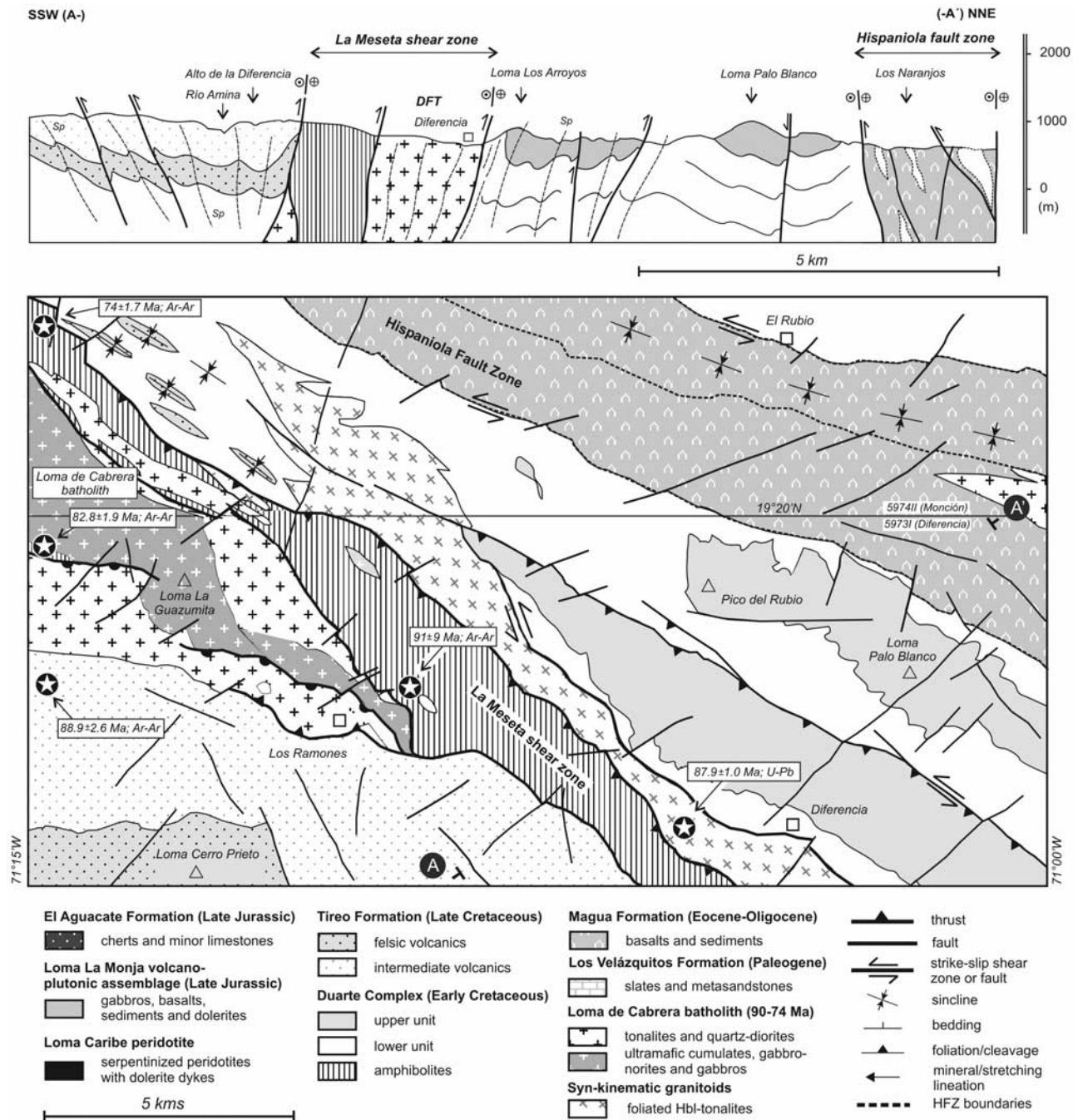


Figure 2. Schematic geological map and A-A' geological cross section through the El Rúbio-Diferencia area showing the stratigraphic and structural relationships between the Duarte Complex and other units of the Cordillera Central.

with the Magua-Tavera Formation (Figures 2 and 3) and unconformably deposited over these units, indicates that the main structure of central Hispaniola was pre-Eocene/Oligocene.

[10] In the study area of Cordillera Central, five lithostratigraphic and geochemical units have been mapped [Contreras et al., 2004; Joubert et al., 2004]. They include, from bottom to top (Figure 4): (1) the Loma Caribe serpentinized peridotite; (2) the Loma La Monja volcano-plutonic assemblage; (3) the El Aguacate Chert; (4) the Duarte Complex; and (5) the Tireo Formation. All these

units underwent variable deformation and low-grade metamorphism. The Loma Caribe serpentinized peridotite consists of serpentinized harzburgite, dunite and lherzolite, with dikes and tectonic blocks of gabbro and dolerite. The Loma La Monja volcano-plutonic assemblage consists of a <3-km-thick sequence of isotropic gabbros, minor cumulate-layered olivine gabbros, massive Fe-Ti basalts and dolerites that grade upward into pillow lavas and pillow breccias, and are overlain by phryic basalts, tuffaceous sediments and the El Aguacate Chert. The El Aguacate Chert consists of about 150-m-thick sequence of ribbon

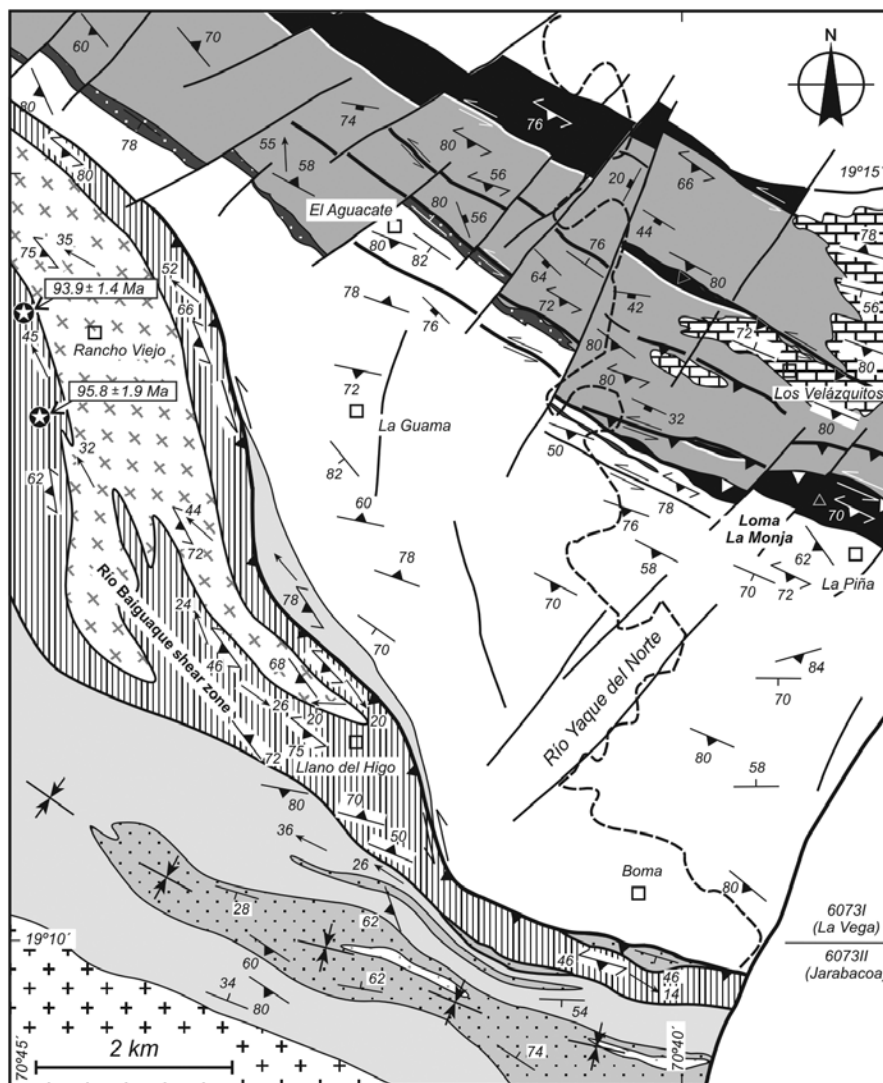


Figure 3. Schematic geological map of the southwest La Vega area, Cordillera Central (modified from Lewis and Jiménez [1991]). Stars show locations of samples for Ar-Ar geochronology and obtained ages.

chert with locally interlayered thin-bedded limestone. Radiolarian microfauna provided an Oxfordian to Tithonian age [Montgomery *et al.*, 1994]. Duarte Complex-like mafic dikes cut the Loma La Monja volcano-plutonic assemblage and the El Aguacate Chert. The Tiroe Formation consists of >3 km thick sequence of arc-related volcanic, subvolcanic, and volcano-sedimentary rocks of Cenomanian to Maastrichtian age [Lewis and Jiménez, 1991], that overlie unconformably the Duarte Complex. The basal unit of El Yujo consists of 20–35 m of interbedded fine-grained tuff, shale, limestone and ribbon chert, overlain by rhyolitic flows. The island arc magmatism finished prior to mid-Eocene, as recorded by the deposition of shallow water limestone (Nalga de Maco Formation) of middle to late Eocene age on top of the arc volcanics.

3. Duarte Complex: Field Relations and Petrography

[11] The macrostructure of the Duarte Complex in the study area consists of several WNW trending blocks

bounded by subvertical or SW dipping ductile shear zones and ductile-brittle strike-slip faults, which can be up to 3 km wide, and internally deformed by a system of open, sub-vertical folds (Figure 2). In the metavolcanic rocks, the deformation is heterogeneous and related to strain and thermal gradients, which are expressed macroscopically by a variably penetrative foliation. In low-strain sectors located between the shear zones where regional metamorphism was static, the textures and relic mineralogy in the volcanic protoliths are often preserved. Two sectors are key to investigate the field relations (Figures 2 and 3): the El Rubio-Diferencia and southwest La Vega area. In both sectors, two main lithostratigraphic units have been mapped in the Duarte Complex (Figure 4), which is unconformably overlain by the Tiroe Formation in WNW trending synclines.

[12] The lower unit is dominated by massive and banded flows of olivine and pyroxene porphyritic picrite, and aphyric olivine basalt, locally capped by autoclastic breccias and intruded by synvolcanic dikes and sills of basalt and dolerite. Picrites are present through the entire volcanic

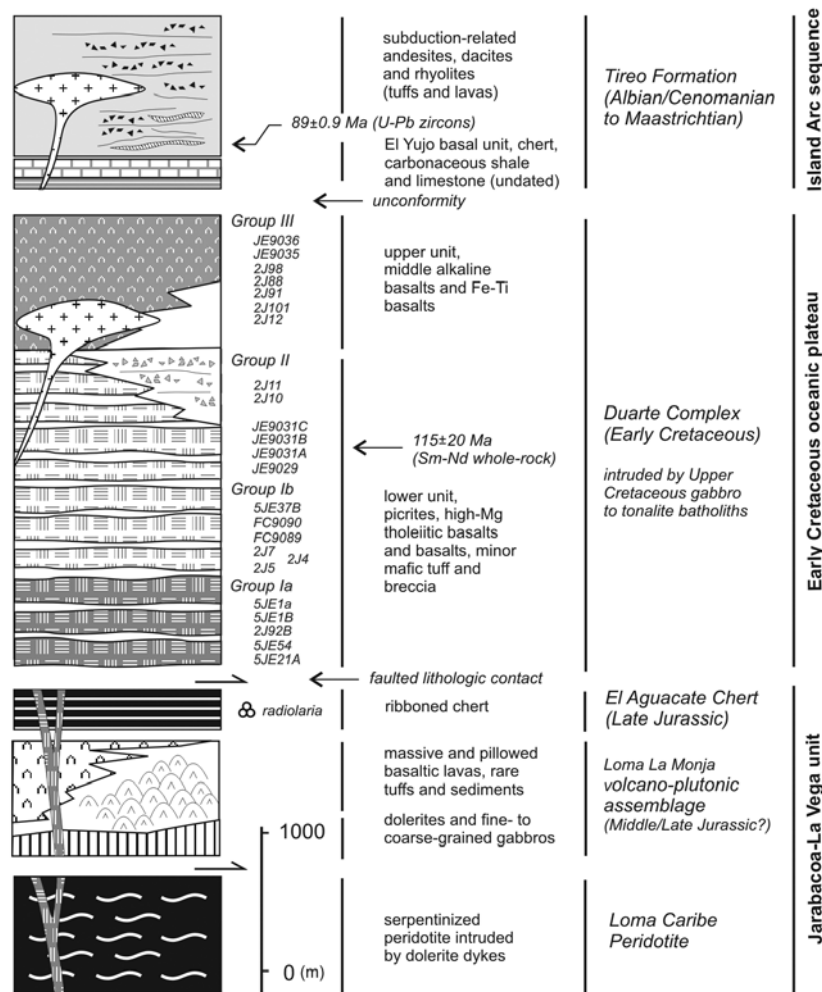


Figure 4. Schematic lithostratigraphic column of the Duarte Complex showing the location of the samples collected for this study.

section. These rocks were extruded in a deep submarine environment at high effusive rate indicated by the scarcity of intercalated pelagic sediments. Toward the top of the unit, lava flows locally grade to tuff breccias, occasionally with chert and picrite clasts, probably resulting from explosive volcanism caused by the contact between magma, water and sediments. The presence of these breccias on top of the lava pile suggests that eruptions may have occurred in shallower water; nevertheless, no evidence of subaerial eruptions has been found. A massive and homogeneous ~ 1.5 -km-thick pile of basaltic submarine flows with sparse interlayered carbonate pelagic sediments, and rare intrusions of synvolcanic mafic dikes compose the upper unit. Typically, basalts are bluish gray to dark gray, aphyric, and rarely amygdalar.

[13] Texturally, picrites are dark green to brown, mostly porphyritic and rarely aphyric. They consist of up to 60% pseudomorphosed olivine and clinopyroxene phenocrysts, 1–6 mm in diameter, set in a recrystallized, quenched groundmass. Euhedral dark brown Ti-rich Cr-spinel occurs mainly as inclusions in olivine. Aphyric picrites show fine-grained intergranular, or subophitic textures. The high modal abundance of phenocrysts in picrites suggests a cumulate origin. Occasionally preserved intercumulus

plagioclase shows that olivine and clinopyroxene, together with spinel, preceded plagioclase in the crystallization sequence. High-Mg basalts and dolerites consist of olivine, clinopyroxene, and plagioclase microphenocrysts and late crystallizing Fe-Ti oxide grains. Plagioclase may form glomeroporphyritic clusters. Where visible, groundmass textures range from ophitic/subophitic to very fine grained granular. All these rocks were affected by mostly pervasive alteration/metamorphism: olivine was replaced by Mg-chlorite, clinopyroxene by Ca-amphibole \pm epidote, and plagioclase by albite \pm white mica \pm calcite \pm prehnite. The upper unit basalts are aphyric, with fine-grained intersertal to subophitic textures, or microporphyritic with plagioclase and clinopyroxene phenocrysts, and a microgranular groundmass composed of plagioclase, clinopyroxene, abundant Ti magnetite, and secondary minerals. In foliated rocks, a tectonometamorphism in the prehnite-pumpellyite to greenschist facies conditions was developed and recorded by stable mineral assemblages in the foliation planes of prehnite + pumpellyite + albite + Fe-rich epidote \pm white mica and actinolite/actinolitic hornblende + albite + epidote + chlorite + white mica \pm sphene \pm quartz, respectively. Synkinematic, amphibolite facies assemblages were also developed in the Duarte Complex rocks along shear zones

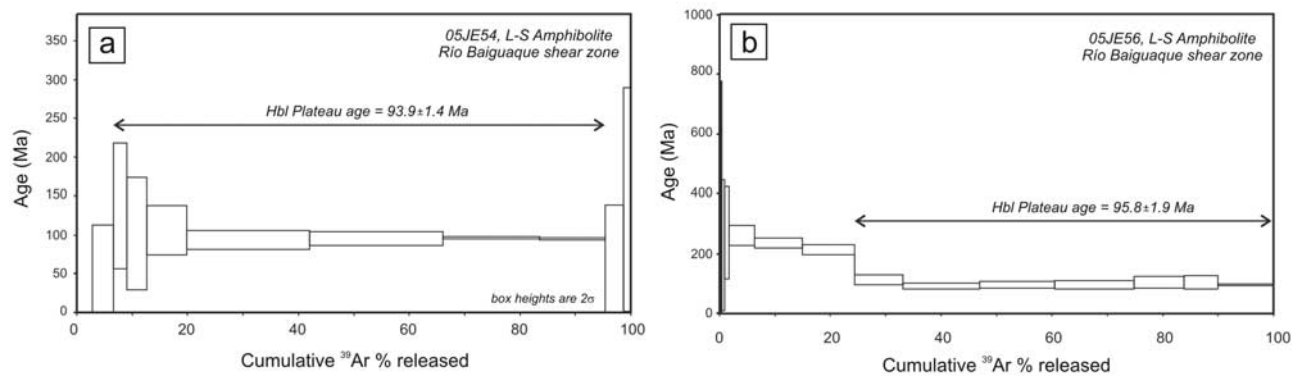


Figure 5. The $^{40}\text{Ar}/^{39}\text{Ar}$ spectrum of hornblende in blastomylonitic S-L amphibolites from the Río Baiguaque shear zone (samples 05JE54 and 05JE56). See text for discussion.

related with the emplacement of tonalite, as the amphibolites of the La Meseta and Río Baiguaque shear zones (Figures 2 and 3).

4. The $^{40}\text{Ar}/^{39}\text{Ar}$ Geochronology

4.1. Results

[14] Two amphibolites of the Duarte Complex were selected for $^{40}\text{Ar}/^{39}\text{Ar}$ analysis (Figure 3) with the aim of dating the age of the tectonometamorphism. The used methodology and the complete data set of the incremental heating $^{40}\text{Ar}/^{39}\text{Ar}$ experiments are included in Tables S1 and S2 in the auxiliary material.¹ Both samples show a planar fabric with a strong mineral lineation defined by 0.5–1.5 mm long hornblende nematoblasts that support the simultaneity of ductile deformation and amphibolite facies metamorphism. Sample 05JE54 is a blastomylonitic amphibolite from the Río Baiguaque shear zone. As indicated by its geochemistry, the protolith was a picrite from the lower unit of Duarte Complex. The obtained hornblende plateau age is 93.9 ± 1.37 Ma for seven steps (3–9) and 93.9% of the ^{39}Ar released (Figure 5a). Normal and inverse isochron ages are 94.5 ± 5.2 Ma and 92.4 ± 8.4 Ma, respectively. Sample 05JE56 is also a foliated amphibolite from the Río Baiguaque shear zone. The protolith was tholeiitic basalt. The obtained hornblende plateau age is 95.8 ± 1.9 Ma for seven steps (7–14) and 95.8% of the ^{39}Ar released, and the inverse isochron age is 91.5 ± 12.6 Ma (Figure 5b).

4.2. Interpretation

[15] The two $^{40}\text{Ar}/^{39}\text{Ar}$ hornblende plateau ages obtained from amphibolites of the Duarte Complex overlap within analytical uncertainties. These Late Cenomanian ages (time-scale from *Gradstein et al.* [2004]) are interpreted as the age of the metamorphic peak, due to the closure temperature of hornblende (525–450°C) and the temperatures of 548–472°C obtained from Hbl-Pl thermobarometry of the analyzed amphibolites. Moreover, given that hornblende defines the S-L fabric and grew simultaneously with shearing, the obtained ages also date the Río Baiguaque shear zone that affected both units of the Duarte Complex.

Therefore an older, pre-Cenomanian age of the igneous protoliths of the Duarte Complex is inferred. Probably, the $^{40}\text{Ar}/^{39}\text{Ar}$ cooling ages of 87–86 Ma obtained on undeformed picrite and amphibolite by *Lapierre et al.* [1999] are the age of the same regional tectonometamorphic event, developed in static conditions out of the ductile shear zones.

[16] Evidence that support an Early Cretaceous age for the Duarte Complex come from regional stratigraphic, geochronological, and structural data. Folding and thrusting of the Tiroo Formation in the northern domain of the El Rubio-Diferencia sector (Figure 2) is later than the U-Pb ages of intrusive, arc-related dacite (91.8 ± 2.3 Ma) and rhyolite (91.3 ± 2.1 Ma) [*Joubert et al.*, 2004]. These ages are consistent with the Albian to Upper Cenomanian paleontological age, obtained from foraminifera in the Tiroo Formation by *Montgomery and Pessagno* [1999]. U-Pb zircon analysis of plutonic rocks from the Macutico batholith, yielded a crystallization age of 90.0 ± 1.9 Ma for a diorite, and 92.1 ± 1.2 Ma for a tonalite [*Contreras et al.*, 2004]. These authors argue that arc-related dacite and rhyolite of the Tiroo Formation are the extrusive equivalent of the diorite and tonalite intrusives. This, together with the 87.9 ± 1.0 Ma U/Pb zircon age of the tonalite intrusive along the La Meseta shear zone at Diferencia (MJ9195, Figure 2 [*Joubert et al.*, 2004]), shows that shearing of the Tiroo Formation occurred at least from 92–88 Ma (Turonian-Coniacian) and constrains the age of the underlying Duarte Complex to being older than 92 Ma. This is consistent with the whole rock Sm/Nd isochron age of 115 ± 20 Ma (MSWD = 1.15; $^{143}\text{Nd}/^{144}\text{Nd}_i = 0.512826$) obtained from eight samples of picrites and high-Mg basalts of the Duarte Complex [*Escuder-Virquete et al.*, 2004]. In conclusion, the Duarte Complex volcanic rocks were extruded during the Early Cretaceous, in pre-Cenomanian, probably Aptian time.

5. Geochemistry

5.1. Alteration and Tectonometamorphism

[17] Duarte Complex rocks have been variably altered, deformed and metamorphosed. Consequently, changes of the bulk rock chemistry are expected as a consequence of selected mobility of relevant elements. It is known that some major (e.g., Si, Na, K, Ca) and trace (e.g., Cs, Rb, Ba, Sr) elements are easily mobilized by late and/or postmagmatic

¹Auxiliary materials are available at <ftp://ftp.agu.org/apend/jb/2006/jb004323>.

Table 1. Whole Rock Geochemical Data for the Duarte Complex^a

	Group Ia						Group Ib						Group II						Group III											
	HMB		BAS		ANF		PIC		HMB		FC9089		HMB		PIC		JE9031B		JE9031C		JE9031A		BAS		FBAS		BAS			
	5JE21a	5JE01b	5JE54	5JE54	02192B	ANF	FC9090	5JE37b	FC9089	0215	0214	0217	JE9029	JE9031B	JE9031C	JE9031A	02J10	02J11	02J18	JE9035	02J91	JE9036	02J12							
X (UTM)	327223	323670	314509	320437	279312	323762	279246	280120	280120	280120	280250	281619	281941	281941	281941	281941	280200	280200	279000	316100	316100	280981	280700	280700	280700	280700	280700	280700	280700	
Y (UTM)	2124077	2124810	2130479	2121401	2139172	2125086	2139659	2138700	2138700	2138700	2138800	2139103	2137934	2137934	2137934	2138900	2138900	2137000	2129400	2129400	2129500	2136030	2135500	2135500	2135500	2135500	2135500	2135500	2135500	
	Major Oxides, wt %																													
SiO ₂	48.88	49.60	49.26	48.21	45.74	48.29	48.58	47.73	48.35	49.42	44.97	47.71	48.25	47.29	48.47	48.72	49.60	48.17	49.17	49.17	49.13	56.02	56.02	56.02	56.02	56.02	56.02	56.02	56.02	56.02
TiO ₂	1.26	1.06	1.59	1.74	2.50	2.08	2.60	2.21	2.25	2.59	1.68	1.64	1.61	2.09	3.24	1.99	3.94	3.54	4.00	4.00	3.45	2.49	2.49	2.49	2.49	2.49	2.49	2.49	2.49	
Al ₂ O ₃	10.28	8.16	12.36	13.87	8.12	7.55	8.93	8.87	9.02	9.26	9.07	9.59	9.50	10.28	11.18	12.59	13.79	13.31	13.75	13.75	13.30	13.91	13.91	13.91	13.91	13.91	13.91	13.91	13.91	
Fe ₂ O _{3T}	12.39	11.17	12.13	12.82	13.00	12.72	12.75	13.21	13.09	13.20	15.35	14.18	13.82	14.37	14.95	15.20	13.13	13.96	13.77	13.77	13.86	11.88	11.88	11.88	11.88	11.88	11.88	11.88	11.88	
MgO	15.41	13.93	10.90	7.61	20.99	18.31	16.20	17.25	16.18	15.37	18.25	14.31	13.98	13.25	8.97	7.14	6.42	6.75	6.27	6.30	6.27	6.30	4.24	4.24	4.24	4.24	4.24	4.24	4.24	
CaO	8.65	14.85	10.37	12.44	8.09	9.86	9.05	9.19	9.08	8.48	9.34	9.65	9.75	9.70	9.36	10.69	10.35	10.86	9.63	9.63	9.44	7.39	7.39	7.39	7.39	7.39	7.39	7.39	7.39	
Na ₂ O	2.64	0.86	2.84	2.58	0.89	0.62	1.36	0.95	1.35	2.08	0.66	2.22	2.41	2.35	2.75	2.99	2.07	2.56	2.56	2.56	3.48	3.48	3.48	3.48	3.48	3.48	3.48	3.48	3.48	
K ₂ O	0.04	0.12	0.15	0.33	0.05	0.05	0.01	0.06	0.15	0.08	0.08	0.14	0.15	0.15	0.58	0.28	0.07	0.29	0.50	0.50	1.47	1.47	1.47	1.47	1.47	1.47	1.47	1.47	1.47	
P ₂ O ₅	0.07	0.07	0.12	0.18	0.19	0.16	0.21	0.16	0.15	0.18	0.13	0.16	0.14	0.18	0.25	0.19	0.39	0.36	0.35	0.35	0.31	0.25	0.25	0.25	0.25	0.25	0.25	0.25	0.25	
MnO	0.17	0.17	0.15	0.18	0.22	0.16	0.15	0.19	0.19	0.17	0.17	0.19	0.19	0.18	0.22	0.15	0.22	0.16	0.20	0.17	0.17	0.17	0.17	0.17	0.17	0.17	0.17	0.17	0.17	
Cr ₂ O ₃	0.21	0.00	0.11	0.04	0.21	0.20	0.16	0.19	0.19	0.18	0.29	0.22	0.22	0.17	0.02	0.05	0.03	0.04	0.03	0.03	0.03	0.01	0.01	0.01	0.01	0.01	0.01	0.01	0.01	
Total	100	100	100	100	100	100	100	100	100	100	100	100	100	100	100	100	100	100	100	100	100	100	100	100	100	100	100	100	100	
LOI	4.97	0	1.36	0.9	5.3	4.45	4.57	3.65	3.55	3.25	5.8	3.53	3.95	3.31	1.22	0.95	2.45	2.11	1.95	1.95	1.02	0.42	0.42	0.42	0.42	0.42	0.42	0.42	0.42	
Mg # ^c	71	71	64	54	76	74	72	72	71	71	70	67	67	65	54	48	49	49	47	47	47	41	41	41	41	41	41	41	41	
	Minor Oxides, ppm																													
Ni	503	268	50	145	465	491	377	864	699	706	743	465	446	385	40	32	118	134	133	133	107	10	10	10	10	10	10	10	10	10
Cr	1382	1925	766	279	1341	1327	1047	1380	1310	1230	1833	1457	1423	1088	109	322	260	253	227	227	171	48	48	48	48	48	48	48	48	
Co	68.1	-	53.1	50	81.8	75	71	79	72	67	91.8	76.4	80	68.7	53.9	50.9	42	45.6	43	43	49.5	32.9	32.9	32.9	32.9	32.9	32.9	32.9	32.9	
V	258	456	392	431	274	274	267	287	304	301	275	325	336	336	510	398	421	377	433	433	406	386	386	386	386	386	386	386	386	
Rb	1.1	1.8	1.6	4.0	2.1	0.7	<0.5	5.0	7.0	1.0	0.7	0.7	1.1	0.6	17.1	5.4	1.0	3.9	5.0	5.0	22.3	3.1	3.1	3.1	3.1	3.1	3.1	3.1	3.1	
Ba	48.8	23.7	39.5	131	25	16.7	20	30	56	57	10.6	38.6	57.5	44.5	116	161	43	70.9	187	187	431.8	95	95	95	95	95	95	95	95	
Th	0.3	0.2	0.4	1.0	0.9	1.1	1.0	0.8	0.9	1.1	0.7	0.8	0.6	0.8	0.8	0.4	3.3	1.7	3.2	3.2	1.9	1.4	1.4	1.4	1.4	1.4	1.4	1.4	1.4	
U	<1	0.1	0.2	0.2	0.3	0.3	0.2	0.2	0.3	0.3	0.2	0.2	0.3	0.3	0.4	0.3	0.8	0.6	0.7	0.7	0.6	0.5	0.5	0.5	0.5	0.5	0.5	0.5	0.5	
Nb	5.4	3.7	6.7	8.0	13.1	11.7	12.5	11.0	10.0	9.0	9.2	10.5	10.5	13.8	16.9	11.5	27.0	32.1	27.0	27.0	32.6	24.4	24.4	24.4	24.4	24.4	24.4	24.4	24.4	
Ta	0.4	0.2	0.4	0.6	1.0	0.7	0.9	0.8	0.9	0.9	0.5	0.6	0.6	0.6	1.2	0.8	2.3	1.9	2.3	2.3	1.8	1.7	1.7	1.7	1.7	1.7	1.7	1.7	1.7	
La	5.1	3.0	8.0	8.5	9.9	7.2	9.2	7.6	7.4	10.9	6.9	7.5	6.9	10.7	14.8	9.2	22.8	21.3	24.9	24.9	22.3	18.6	18.6	18.6	18.6	18.6	18.6	18.6	18.6	
Ce	12.0	8.2	19.4	19.1	24.1	20.6	24.1	18.5	19.0	26.0	18.5	19.9	18.9	26.7	34.1	22.3	49.7	56.5	56.6	56.6	59.3	34.6	34.6	34.6	34.6	34.6	34.6	34.6	34.6	
Pr	1.8	1.316	2.80	3.12	3.45	2.92	3.31	3.07	3.13	4.23	2.55	2.84	2.65	3.73	4.72	3.23	7.46	7.31	8.31	8.31	7.60	4.30	4.30	4.30	4.30	4.30	4.30	4.30	4.30	
Sr	116.2	114.8	338.5	286.0	76.8	54.0	75.6	104.0	157.0	192.0	59.7	128.6	140.4	184.6	303.3	471.4	364.0	404.3	357.0	357.0	382.4	414.3	414.3	414.3	414.3	414.3	414.3	414.3	414.3	
Nd	9.0	6.9	14.9	15.2	17.6	15.7	18.5	14.6	15.0	19.2	11.8	13.0	12.8	17.1	24.1	18.1	32.7	33.1	36.9	36.9	33.2	21.2	21.2	21.2	21.2	21.2	21.2	21.2	21.2	
Sm	2.5	2.3	4.1	4.6	4.6	4.0	4.7	4.3	4.8	4.9	3.4	3.9	3.5	4.9	7.0	4.4	8.7	7.9	8.6	8.6	8.5	4.3	4.3	4.3	4.3	4.3	4.3	4.3	4.3	
Zr	56	85	80	80	121	99	115	122	128	135	78	81	79	108	138	96	188	201	184	184	207	128	128	128	128	128	128	128	128	
Hf	1.8	0.0	2.6	3.0	3.4	2.9	3.1	3.0	3.0	4.0	2.3	2.5	2.5	3.2	4.6	2.9	6.0	5.7	6.0	5.9	3.2	3.2	3.2	3.2	3.2	3.2	3.2	3.2	3.2	
Eu	0.9	0.80	1.60	1.47	1.65	1.48	1.56	1.49	1.39	1.72	1.16	1.20	1.12	1.54	2.43	1.70	2.93	2.50	2.66	2.53	1.13	1.13	1.13	1.13	1.13	1.13	1.13	1.13	1.13	
Gd	3.01	2.38	4.49	4.67	5.03	4.64	4.69	4.75	4.99	5.31	3.73	3.96	3.77	4.94	6.26	4.98	8.61	7.20	8.53	7.45	3.35	3.35	3.35	3.35	3.35	3.35	3.35	3.35	3.35	
Tb	0.49	0.43	0.73	0.71	0.82	0.64	0.85	0.72	0.79	0.83	0.58	0.64	0.65	0.76	1.10	0.77	1.34	1.19	1.29	1.29	0.64	0.64	0.64	0.64	0.64	0.64	0.64	0.64	0.64	
Dy	2.93	2.56	4.05	4.06	4.51	3.80	4.85	4.21	4.53	4.83	3.18	3.81	3.72	4.49	5.63	3.91	7.27	6.29	6.72	6.72	3.38	3.38	3.38	3.38	3.38	3.38	3.38	3.38	3.38	
Y	16.6	13.2	21.5	19.0	22.9	20.3	24.5																							

Table 2. Sr-Nd Isotope Ratios for Representative Rock Groups of the Duarte Complex^a

Unit	Sample	Rock/Protolith	Type	⁸⁷ Sr/ ⁸⁶ Sr	(⁸⁷ Sr/ ⁸⁶ Sr) _i	(ε _{Sr}) _i	¹⁴³ Nd/ ¹⁴⁴ Nd	(¹⁴³ Nd/ ¹⁴⁴ Nd) _i	(ε _{Nd}) _i
LU	5je21A	high-Mg basalt	type Ia	0.703233 (7)	0.703156	-17.11	0.512977 (9)	0.512819	6.54
LU	FC9089	high-Mg basalt	type Ib	-	-	-	0.512943(6)	0.512822	6.61
LU	FC9090	metapicrite	type Ib	0.703453(8)	0.703318	-14.80	0.512928(7)	0.512804	6.25
LU	02J4	high-Mg basalt	type Ib	0.703380 (8)	0.703352	-14.31	0.512947(6)	0.512817	6.51
LU	JE9029	picrite	type II	0.703388(8)	0.703330	-14.63	0.512944(7)	0.512807	6.32
LU	JE9031A	high-Mg basalt	type II	0.703422(7)	0.703406	-13.56	0.512942(6)	0.512806	6.29
LU	JE9031B	picrite	type II	0.703417(7)	0.703390	-13.78	0.512944 (6)	0.512802	6.21
LU	JE9031C	high-Mg basalt	type II	0.703414(8)	0.703375	-13.99	0.512935 (7)	0.512805	6.28
UU	JE9035	Fe-Ti basalt	type III	0.703467(7)	0.703419	-13.37	0.512862 (6)	0.512749	5.17
UU	JE9036	Fe-Ti basalt	type III	0.703576(7)	0.703288	-15.23	0.512865 (9)	0.512743	5.07

^aLU, lower unit; UU, upper unit. Calculated initial ratios (i) and ε_{Sr} and ε_{Nd} values calculated at *t* = 120 Ma. Number in brackets is the absolute 2σ error in the last decimal places; ε_{Nd} values are relative to ¹⁴³Nd/¹⁴⁴Nd = 0.512638 and ¹⁴⁷Sm/¹⁴⁴Nd = 0.1966 for present-day CHUR and lambda ¹⁴⁷Sm = 6.54 × 10⁻¹²/yr.

processes involving fluids and during metamorphism. However, the concentrations of the high field strength elements (HFSE) Y, Zr, Hf, Ti, Nb and Ta, the rare earth elements (REE), the transition elements V, Cr, Ni and Sc, the large ion lithophile element (LILE) Th, and the Nd isotopic composition are generally unchanged under a wide range of metamorphic conditions, including seafloor alteration [Bienvenu *et al.*, 1990; Bédart, 1999]. In the Duarte Complex samples, relatively immobile trace elements exhibit a good correlation of Zr with Th, Nb, La, Sm, Ti and Yb, with small differences of interelement ratios reflecting primary features that are discussed below. Thus the discussion on the petrogenesis and petrotectonic setting of the Duarte Complex volcanic rocks is based mostly on the REE and HFSE geochemistry, as well as the Sm-Nd isotope systematics, as we can assume that they were not significantly affected by seafloor alteration and tectono-metamorphism at the whole rock scale. Geochemical data are reported in Table 1. A representative suite of samples was also analyzed for Rb-Sr and Sm-Nd isotopic compositions (Table 2). Details of analytical techniques are given in Table S3.

5.2. Whole Rock Compositions

[18] The volcanic rocks of the Duarte Complex range in composition from picrites, containing up to 25 wt % MgO, to high-Mg basalts and basalts (Table 1). These rocks plot in the basaltic komatiite and the high-Fe tholeiite fields of the Fe + Ti-Al-Mg diagram (Figure 6). In Figure 7, selected compatible and incompatible major and trace elements are plotted against MgO, and show a decrease of SiO₂ and TiO₂ (also in Fe₂O_{3T} and alkalis); and an increase in Cr and Ni for increasing MgO. CaO increases slightly to reach a maximum at about 6–7 wt % MgO, then decreases in the evolved basalts. These trends can be attributed to the fractionation and/or accumulation of olivine plus Cr-spinel, clinopyroxene and plagioclase, which is compatible with the relic igneous mineralogy. However, the TiO₂-MgO variation (Figure 7b) shows three distinct trends of low-, intermediate-, and high-Ti rocks, suggesting that these trends are related not only to mineral fractionation/accumulation, but also to distinct, source related, geochemical features of the magmas (see discussion). On the basis of the Nb/Y ratio, the lower and upper unit samples of the Duarte Complex are subalkaline and alkaline basalts, respectively (Figure 8). All samples display a positive Nb (and Ta) and negative Th anomalies in a primitive mantle-normalized extended-REE plot (Figure 9), with LREE enrichment and heavy REE

(HREE)-Y depletion, characteristics of oceanic island basalts.

[19] Initial (⁸⁷Sr/⁸⁶Sr)_i versus (¹⁴³Nd/¹⁴⁴Nd)_i variation of the Duarte Complex is restricted to relatively high (ε_{Nd})_i values between +6.6 and +5.0 (where *i* = 120 Ma; Figure 10a and Table 2), but in the range of ocean island basalts [Weis *et al.*, 2001]. (⁸⁷Sr/⁸⁶Sr)_i ratio values are very homogeneous (0.70315 to 0.70340), near a MORB array calculated at *t* = 120 Ma, which probably reflects their source composition, little modified by minor, subsolidus, hydrothermal alteration. However, the comparison of samples of the Duarte Complex with similar degrees of fractionation (wt % MgO or Mg #) reveals considerable variation in the trace element ratios (Figure 8), the patterns on primitive mantle normalized extended REE plots (Figure 9) and radiogenic isotope ratios (Figure 10). These differences cannot be accounted for by fractional crystallization only, and should therefore result from mantle source heterogeneities, or be caused by differing partial melting processes.

5.3. Discussion

5.3.1. Chemical Classification

[20] To address mantle melting and source variability in oceanic basalts, the ratios of incompatible trace elements unaffected by the addition or removal of olivine, i.e., Nb/Y,

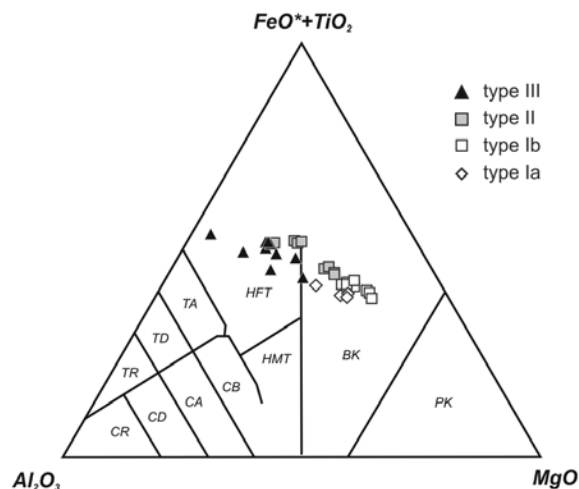


Figure 6. Fe + Ti-Al-Mg plot [Jensen, 1976] for the geochemical groups of the Duarte Complex defined in the text.

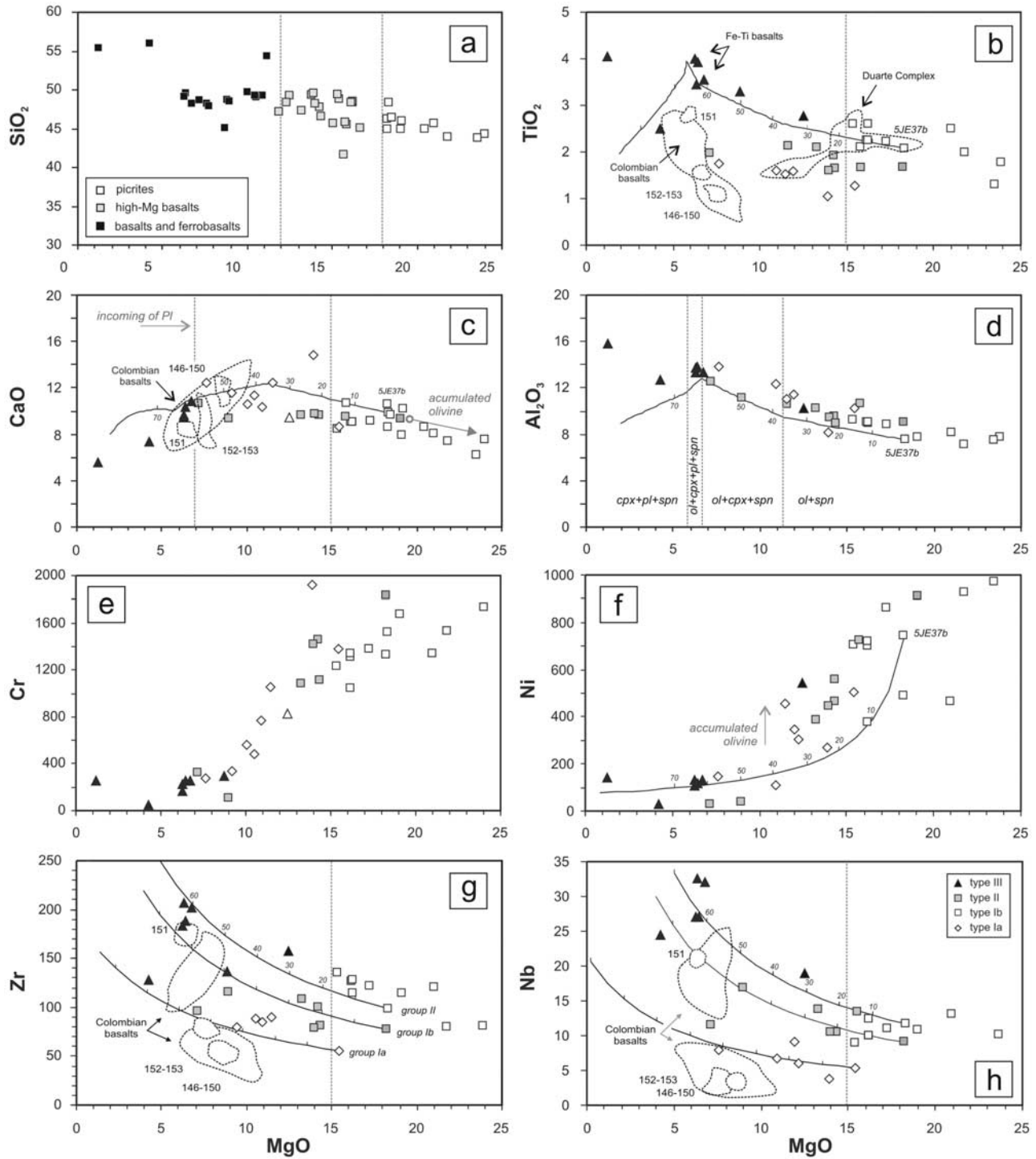


Figure 7. Plots of selected major and trace elements against MgO of picrites, high-Mg basalts and basalts from the Duarte Complex. In Figure 7b the fields of CCOP samples from Sites 146, 150, 151, 152 and 153 of DSDP Leg 15, and Colombian basalts [Kerr *et al.*, 1997a, 2002] are shown for comparison with the Duarte Complex. Data from *Lapierre et al.* [1997] are also included. The vertical dashed line in Figures 7b, 7c, 7g, and 7h indicates the estimated MgO of primitive magma from the Duarte Complex lavas (see text). Major (Figures 7b, 7c, and 7d), metal (Figures 7e and 7f) and trace element (Figures 7g and 7h) modeled fractional crystallization trends using PELE program [Boudreau, 1999] for three representative starting compositions 5JE21a (type Ia), 5JE37b (type Ib) and JE9029 (type III) are also shown. Ticks on the trends represent 10% crystallization intervals. Figure 7d includes the modeled sequence of crystallizing phase assemblages at wt % MgO intervals for type Ib 5JE37b sample.

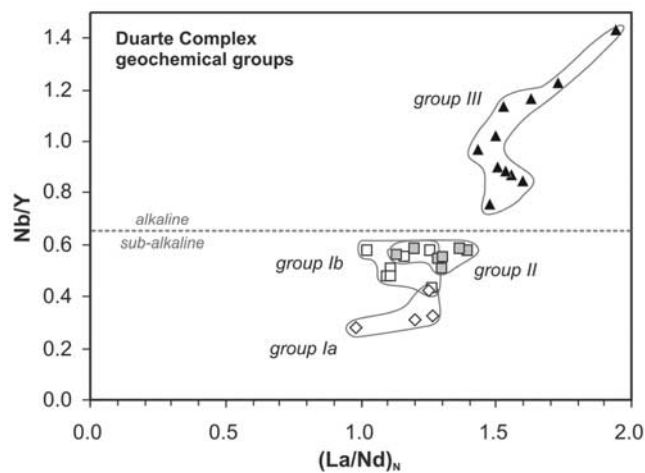


Figure 8. Plot of primitive mantle-normalized $(\text{La}/\text{Nd})_N$ (normalizing values from *Sun and McDonough* [1989]) versus Nb/Y of picrites, high-Mg basalts and basalts of the Duarte Complex.

$(\text{Sm}/\text{Yb})_N$ and $(\text{La}/\text{Nd})_N$ [Fitton *et al.*, 1997; Kerr *et al.*, 1997a, 2002] are useful, because these ratios have the potential to reveal either the chemistry or the mineralogy of the source region, $(\text{La}/\text{Nd})_N$ the LREE depletion or enrichment, Nb/Y and $(\text{Sm}/\text{Yb})_N$ the presence of garnet. On the basis of these ratios and TiO_2 content (Figure 11), the analyzed samples of the Duarte Complex can be divided into four geochemical groups, with probably transitional compositions: group Ia, low-Ti high-Mg basalts; group Ib, high-Ti picrites and unfractionated high-Mg basalts; group II, LREE-enriched picrites, ferropicrites and high-Mg basalts; and group III, LREE-enriched high-Ti basalts (Fe-Ti basalts). In the lithostratigraphy of the Duarte Complex (Figure 4), groups Ia and Ib occur interlayered in the lowermost levels of the lower unit, group II forms the main lava sequence of the lower unit, and group III appears exclusively in the upper unit.

[21] Group Ia of low-Ti high-Mg basalts is represented by the mafic flows and monogenetic autoclastic breccias of the lowermost Duarte Complex. These rocks plot in the basaltic komatiite field of the Fe + Ti-Al-Mg plot (Figure 6) and are unfractionated to slightly fractionated with Mg # ranging from 71 to 54. TiO_2 ranges between 1.0 and 1.7 wt % (Table 1 and Figure 7b), Zr is over 55 ppm and Nb 5 ppm at 15 wt % MgO. Cr (1925–275 ppm) and Ni (500–50 ppm) are lower than those of other rock groups (Figures 7e and 7f). The extended-REE patterns (Figure 9a) are similar to modern tholeiitic ocean island basalts [e.g., Frey *et al.*, 2002] having similar, 4 to 11 times primitive mantle, LREE abundance, flat to slightly LREE-enriched REE patterns ($[\text{La}/\text{Nd}]_N = 0.98$ –1.5; Figure 11), small positive Nb anomaly ($\text{Nb}/\text{Y} < 0.45$; Figure 8), small negative Zr anomaly, and depletion in HREE and Y ($[\text{Sm}/\text{Yb}]_N = 1.9$ –3.0). The initial ratio $(^{87}\text{Sr}/^{86}\text{Sr})_i$ of sample 5JE21a is 0.70316 (Table 2). The $(\epsilon_{\text{Nd}})_i$ value is +6.54, which suggests a dominant depleted mantle source with a HREE depletion.

[22] Group Ib of high-Ti picrites and unfractionated high-Mg basalts is represented by the mafic banded and massive flows, cumulates, autoclastic breccias and minor

synvolcanic intrusions of the lowermost Duarte Complex. These rocks plot in the basaltic komatiite field and are unfractionated (Mg # = 76–71), with relatively high TiO_2 that ranges from 2.1 to 2.6 wt %. Concurrently, they contain over 130 ppm Zr and over 10 ppm Nb at 16 wt % MgO. Cr (1375–1050 ppm) and Ni (850–375 ppm) are higher than those of other rock groups. The extended REE patterns (Figure 9b) are similar in the analyzed samples, and differ from those of group Ia basalts in higher Ti, and absolute REE abundance (LREE 10 to 15 times primitive mantle) for the same Mg #. These picrites and basalts show REE patterns that are flat to slightly LREE-enriched ($[\text{La}/\text{Nd}]_N = 1.0$ –1.26) and HREE (and Y)-depleted ($[\text{Sm}/\text{Yb}]_N = 2.8$ –3.1). Moreover, they have positive Nb anomaly ($0.48 < \text{Nb}/\text{Y} < 0.57$), and slightly negative or positive Zr (and Hf) anomalies. Average $(^{87}\text{Sr}/^{86}\text{Sr})_i$ ratio is 0.7033 ± 0.00002 . The $(\epsilon_{\text{Nd}})_i$ values range from +6.2 to +6.6 suggesting a source dominated by depleted mantle.

[23] Group II is dominated by (meta) picritic, ferropicritic (>15 wt % FeO_T) and ankaramitic cumulates, and high-Mg basaltic lavas, locally capped by brecciated flows, interbedded in the lower unit. These rocks plot range from the basaltic komatiite to high-Fe tholeiite fields and extend to more fractionated compositions (Mg # from 70 to 48) than groups Ia and Ib. TiO_2 ranges between 1.6 and 2.1 wt %, and is higher than that of group Ia for the same MgO content. Zr is over (108–80 ppm) and Nb over 14–10 ppm at 15 wt % MgO. The less fractionated group II rocks are high in Cr (1825–300 ppm) and Ni (750–40 ppm). The extended-REE patterns (Figure 9c) are similar in the analyzed samples, strongly enriched in LREE ($[\text{La}/\text{Nd}]_N = 1.2$ –1.4) and depleted in HREE ($[\text{Sm}/\text{Yb}]_N = 2.4$ –3.4), with positive Nb ($0.58 > \text{Nb}/\text{Y} > 0.54$) and negative Th anomalies. Average $(^{87}\text{Sr}/^{86}\text{Sr})_i$ ratio is 0.70338 ± 0.00003 . $(\epsilon_{\text{Nd}})_i$ ranges from +6.2 to +6.3, compatible with a source dominated by depleted mantle. The higher TiO_2 and $[\text{Sm}/\text{Yb}]_N$ ratios suggest that the mantle source for group II rocks was more enriched than for group Ia.

[24] Group III of LREE-enriched high-Ti basalts (Fe-Ti basalts) is represented by homogeneous, aphyric, midalkaline lavas of the upper unit of the Duarte Complex. The rocks plot in the high-Fe tholeiite field and include the more fractionated compositions of all sampled rocks (Mg # from 62 to 41). They are high in TiO_2 (2.8–4.0 wt %), and Fe_2O_{3T} (11.8–15.2 wt %), and are therefore classified as Fe-Ti basalts. They contain over 169 ppm Zr and over 120 ppm Nb at 12.5 wt % MgO. The more compatible trace elements show a wide range of values, 850–50 ppm for Cr, and 550–10 ppm for Ni. For similar Mg #, these rocks have higher LREE and HREE abundances than group II (Figures 9d and 9e). They have strongly LREE enriched patterns ($[\text{La}/\text{Nd}]_N = 1.4$ –2.0) and depleted HREE ($[\text{Sm}/\text{Yb}]_N = 3.0$ –3.9), with variable positive Eu and Ti anomalies related to plagioclase and Fe-Ti oxide accumulation. This pattern and $\text{Nb}/\text{Y} > 0.9$ values are characteristics of modern-day alkalic oceanic island basalts [Frey *et al.*, 2002]. Average $(^{87}\text{Sr}/^{86}\text{Sr})_i$ ratio is 0.70335 ± 0.00009 . The lowest positive $(\epsilon_{\text{Nd}})_i$ values of +5.07 and +5.17 obtained in group III rocks are compatible with a depleted mantle source, but slightly more enriched than for group I and II (or a less degree of partial melting). Though group III samples appear to correspond to the evolved

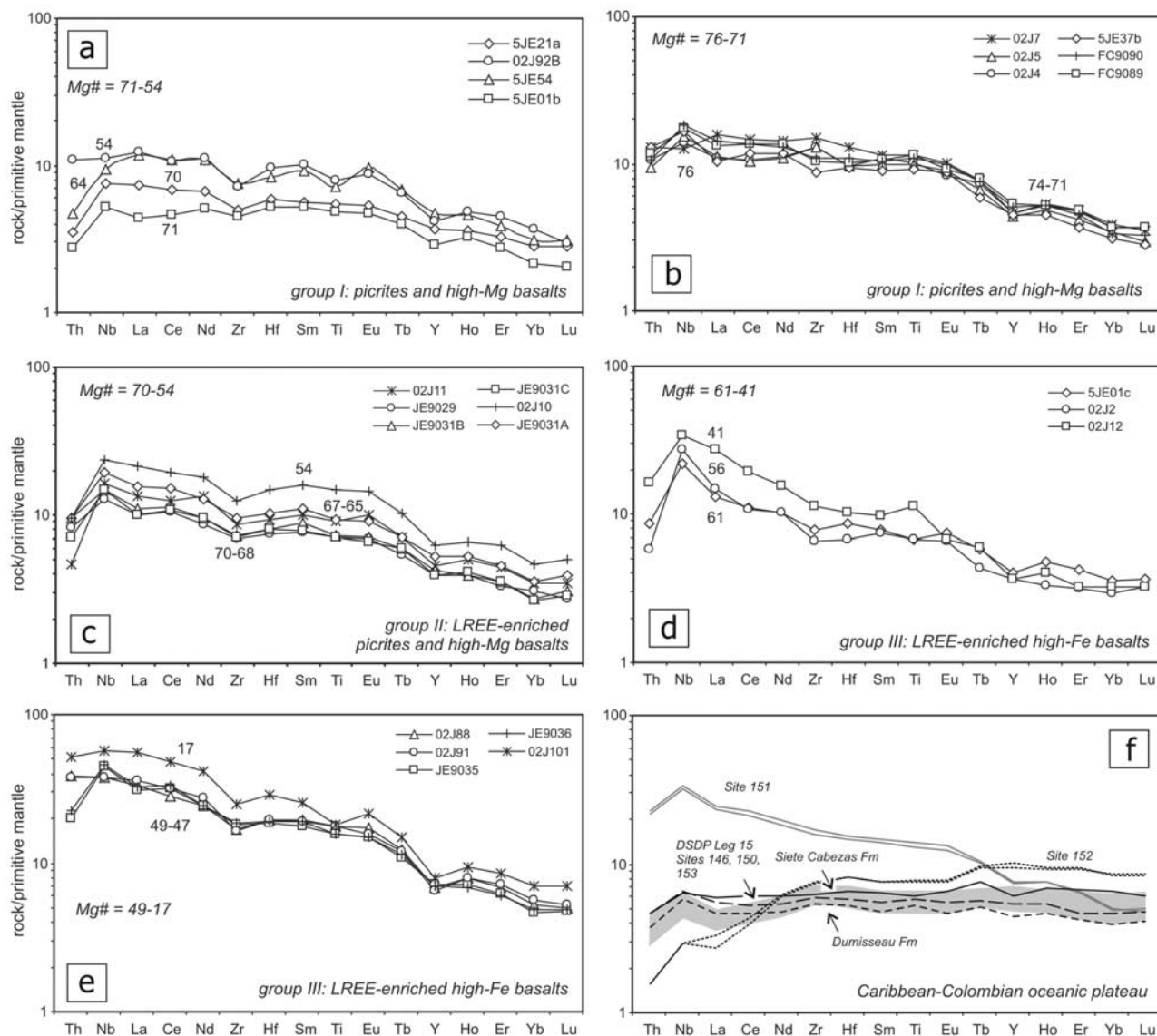


Figure 9. Primitive mantle-normalized extended REE diagrams, showing the patterns of Duarte Complex rocks with different Mg # (Table 1). Four geochemical groups are distinguished: (a) group Ia, low-Ti high-Mg basalts; (b) group Ib, high-Ti picrites and unfractionated high-Mg basalts; (c) group II, LREE-enriched picrites, ferropicrites and high-Mg basalts; and (d, e) group III, LREE-enriched high-Ti basalts (Fe-Ti basalts). In Figure 9e, CCOP basalts from DSDP Leg 15, Dumisseau Formation (Haiti) and Siete Cabezas Formation (Dominican Republic) are included for comparison (compiled by *Sinton et al.* [1998]). Primitive mantle-normalizing values are from *Sun and McDonough* [1989].

melts of group Ib by fractional crystallization along an high-Ti trend in Figure 7b, the different stratigraphic position and trace element and isotopic ratios argue against a genetic link between these two groups.

5.3.2. Evidence of Olivine Accumulation in the High-Mg Rocks

[25] Field and petrographic observations in high-Mg rocks of the Duarte Complex suggest that they are crystal cumulates of olivine. Using the compositions of olivine phenocrysts and relations between major oxides and Ni, *Spadea et al.* [1989] and *Révilion et al.* [2000] estimated compositions of parental liquids in picrites and high-Mg basalts of the CCOP. They estimated a 12–18 wt % MgO

content of the primary mantle melt, and thus samples with >18–20 wt % MgO contain accumulated olivine phenocrysts. For analyzed olivine compositions of Fo_{90-86} , similar calculations suggest that the picrites with 20–25 wt % MgO contain 20–40 vol % accumulated olivine. In light of these observations, we have attempted to reproduce the composition of the Duarte Complex lavas using the PELE software of *Boudreau* [1999]. Given a starting magma composition, PELE calculates mineral and residual magma compositions during fractional crystallization based a free energy minimization technique. The starting magma compositions representative of each TiO_2 group were: a low-Ti high-Mg basalt containing 15.4 wt % MgO (5JE21a); a slightly more

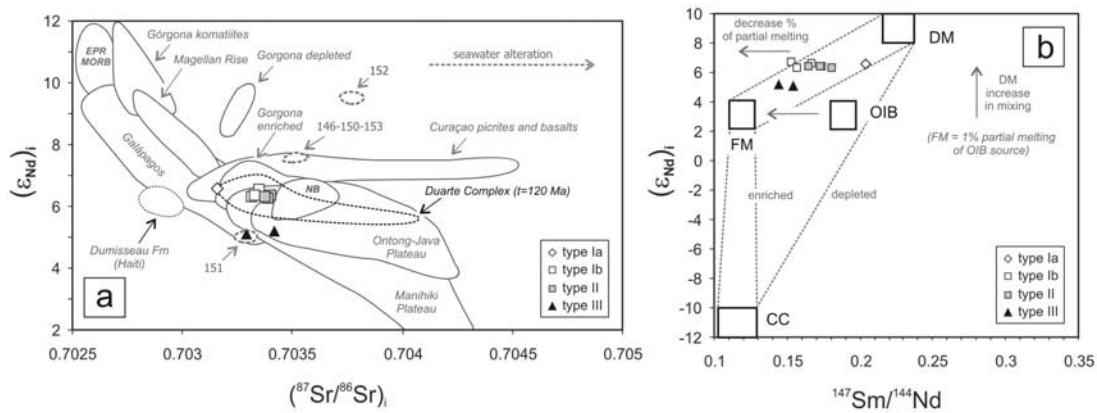


Figure 10. (a) Initial Sr-Nd isotope ratios of the Duarte Complex samples. Initial ratios (i) and $(\epsilon_{Nd})_i$ values were at $t = 120$ Ma. The fields for CCOP samples from the Duarte Complex, Dumisseau Formation, DSDP Leg 15 Sites, Curaçao, Gorgona, and Galápagos, as well as from the East Pacific Rise (EPR MORB), Magellan Rise, and Nauru Basin, Ontong-Java and Manihiki Pacific oceanic plateaus, are taken from Arndt et al. [1997], Hauff et al. [2000a, 2000b], Kerr et al. [1996, 1997a, 2002], Lapierre et al. [1997], and Sen et al. [1988]. (b) The $^{147}\text{Sm}/^{144}\text{Nd}$ versus $(\epsilon_{Nd})_i$ diagram for the same rocks showing the various end-member mantle components interpreted to be involved in its petrogenesis. Following the methodology described by Swinden et al. [1990], hypothetical mantle sources are DM (depleted mantle; i.e., MORB-like source); OIB (ocean island basalt source); FM (fertile mantle, interpreted as a 1% partial melt of OIB); and CC (continental crust or subducted continental material). Dashed lines illustrate schematically mixing trends. See text for explanation.

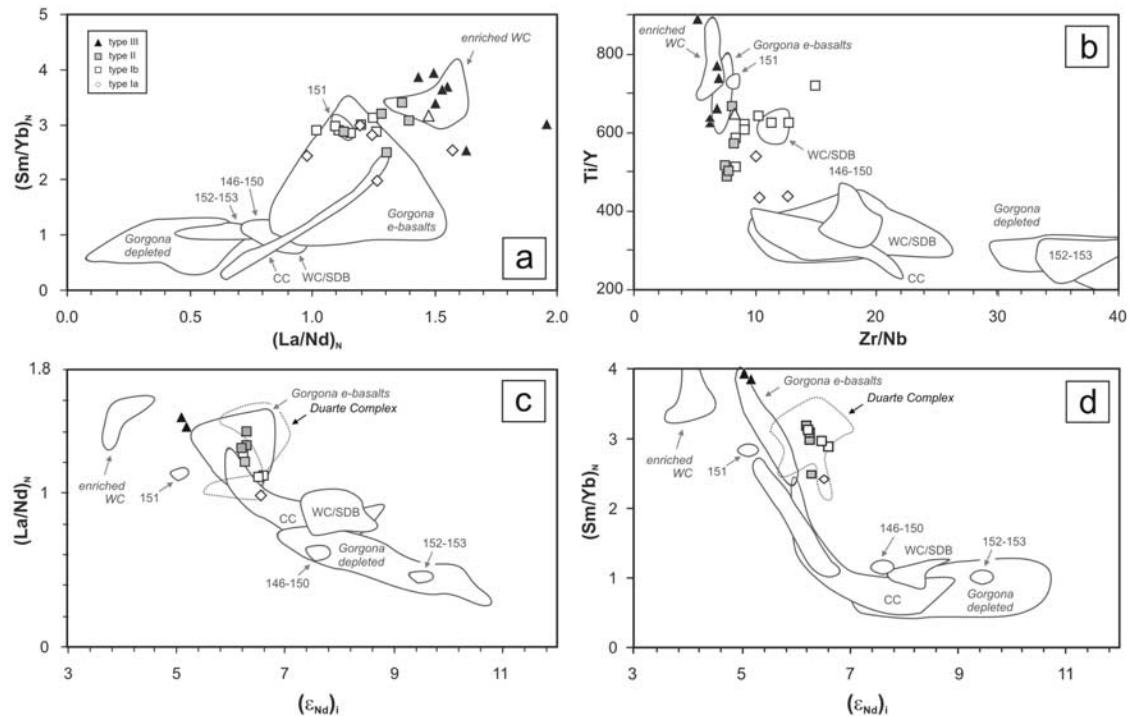


Figure 11. Plots of (a) $(\text{La}/\text{Nd})_N$ versus $(\text{Sm}/\text{Yb})_N$; (b) Zr/Nb versus Ti/Y ; (c) $(\epsilon_{Nd})_i$ versus $(\text{La}/\text{Nd})_N$; and (d) $(\epsilon_{Nd})_i$ versus $(\text{Sm}/\text{Yb})_N$ of the Duarte Complex rocks. Subscript i denotes age corrected initial values at 120 Ma. The fields for CCOP samples from the Duarte Complex (c, d), DSDP Leg 15 (Sites 146, 150, 151, 152 and 153), Central Cordillera (CC), Western Cordillera/Serranía de Baudó (WC/SDB) Colombian basalts, and Gorgona e-basalts and depleted basalts, komatiites and picrites are taken from Arndt et al. [1997], Kerr et al. [1996, 1997a, 2002] and Lapierre et al. [1997].

Ti-enriched picrite containing 18.2 wt % MgO (JE9029); and a high-Ti picrite containing 18.3 wt % MgO (5JE37b). The residual magma compositions obtained from modeling are shown in Figure 7. In all three models, the first phase to crystallize is olivine (+Cr-spinel), followed in the fractionating assemblage by clinopyroxene, then plagioclase and finally Fe-Ti oxide. For the high-Ti 5JE37b starting composition, for example, ol+spl, ol+cpx+spl, ol+cpx+pl and cpx+pl+Fe-Ti oxide assemblages crystallize at >11.4, 11.4–5.8, 5.8–5.0 and <5.0 wt % MgO intervals, respectively (Figure 7d). The results for Zr and Nb (Figures 7g and 7h) show that the three different “parental magmas” could fractionate to produce the incompatible trace element compositions of most of the Duarte Complex rocks.

5.3.3. Nd and Sr Isotope Variations

[26] In the Duarte Complex, the geochemical groups consisting of relatively enriched and depleted magma groups identified on the basis of their trace element contents and ratios, also possess characteristic radiogenic isotopic ratios. (ϵ_{Nd})_i values tend to decrease upward in the stratigraphic sequence, from group Ia (+6.5) and group Ib (+6.6 to +6.2) picrites and high-Mg basalts, through group II picrites and basalts (+6.3 to +6.2) to the more trace element-enriched group III Fe-Ti basalts (+5.17 to +5.07). The narrow range of (ϵ_{Nd})_i values between +6.6 and 5.0 was also described by *Lapierre et al.* [1997] and indicates a source dominated by depleted mantle. However, LREE-enriched trace element compositions and $^{147}\text{Sm}/^{144}\text{Nd}$ ratios less than expected for depleted mantle, indicate a more fertile component in the mantle source. On a $^{147}\text{Sm}/^{144}\text{Nd}$ versus (ϵ_{Nd})_i diagram (Figure 10b), samples plot above the field for mixing of depleted mantle and continental crust mantle sources, suggesting that the decreasing of (ϵ_{Nd})_i values is not due primarily to the presence of recycled crustal material. The isotopic composition of the samples can be explained by mixing a depleted mantle component (DM, which has long-term LREE depletion) with a fertile mantle component (FM) in variable amounts, following a trend with positive slope on the diagram. An appropriate FM component would have slight to moderate LREE enrichment (i.e., low $^{147}\text{Sm}/^{144}\text{Nd}$ of 0.1–0.13), but positive ϵ_{Nd} values (i.e., long-term history of LREE depletion) about +5 to +7, which was obtained from 1% partial melting of OIB source. Heterogeneous sources for the Duarte Complex are shown in Figure 10b; lower unit samples lie closer to the DM depleted end-member and upper unit samples with more alkaline basalt compositions lie closer to the FM end-member, which is compatible with the geochemical interpretation that they represent melts from a more enriched source (or smaller degrees of partial melting).

6. Petrogenesis and Comparisons

6.1. Mantle Melting and Sources

[27] On the basis of thermodynamic models, experimental petrology, trace element systematics and by analogy with observations of intraoceanic plate hot spots and plateaus, komatiite/picrite and high-Mg tholeiite-dominated volcanic assemblages are widely held to be the product of thermally anomalous deep mantle plumes [*Arndt*, 1999; *Arndt et al.*, 1997; *Kerr et al.*, 1997b; *McDonough and Ireland*, 1993].

In this context, the stratigraphical, geochemical and isotopic data of the Duarte Complex are consistent with the ascending mantle plume model proposed by *Campbell et al.* [1989]. In fact, the relatively depleted group Ia and Ib high-Mg basalts and picrites occur in the lowermost part of the sequence and may derive from upper mantle source containing only small amounts of garnet melted by the initial plume head. The overlying, voluminous group II enriched picrites, ferropicrites and high-Mg basalts of the lower unit may represent hotter parts of the plume head. These melts were later followed by the more enriched group III basalts of the upper unit, which represent plume tail and chemically distinct entrained material. It is likely that evolved group III basalts were mostly derived from more picritic melts which ponded and fractionated deep within the oceanic lithosphere to produce ultramafic cumulates and lower-Mg basaltic liquids, as been proposed by *Kerr et al.* [1997b]. The diversity of magma compositions shown by the Duarte Complex has also been described in other outcrops of the CCOP, including tholeiitic LREE-depleted picrites, komatiites and basalts of Gorgona Island; tholeiitic lavas having flat to slightly LREE-enriched patterns (central and western Colombia), compositionally equivalent to those recovered from Pacific oceanic plateaus; and LREE-enriched, midalkaline basalts (Haiti, western Colombia, 151 site of DSDP Leg 15) that may represent lesser degrees of melting at the cooler periphery of the plume head [*Alvarado et al.*, 1997; *Sinton et al.*, 1998; *Hauff et al.*, 2000a, 2000b; *Kerr et al.*, 1997b, 2002; *Lapierre et al.*, 2000]. This chemical and isotopic diversity in the magmas that generate oceanic plateaus can result from heterogeneity of the plume source region, or be caused by partial melting processes under different conditions (e.g., depth of melting). Source heterogeneity supports the models of *Kerr et al.* [1995, 1997a] and *Arndt et al.* [1997], who proposed that most mantle plumes are heterogeneous, and consist predominantly of a relatively refractory depleted matrix, with a small proportion (<10%) of fusible streaks of more enriched material. Following these models, deep, low-degree mantle melting will preferentially sample these more enriched streaks, whereas at shallow, more extensive melting will produce a greater proportion of magma derived from the depleted matrix.

[28] The Nd isotope and incompatible trace element variations shown in Figure 11 demonstrate that the Duarte Complex igneous rocks derive from a heterogeneous plume source region. As a whole, they are more enriched relative to other CCOP areas, except DSDP Site 151 and El Encenillo lavas from western Colombia. Although Duarte Complex rocks are in general more enriched in incompatible trace elements than CCOP lavas, the positive ϵ_{Nd} values indicate that were derived from a mantle source region with a long-term depletion in the LREE. Thus the variable enriched LREE patterns must represent a relatively recent enrichment, acquired probably during the melting process. The range of $(\text{La}/\text{Nd})_{\text{N}} = 1.0\text{--}1.2$ found in the group I samples (Figure 11c) also reflects the depleted nature of their source region. Nevertheless, this depletion in incompatible trace elements is subtly different in character from that observed, for example, in present-day East Pacific Rise transitional and enriched MORB. In addition, trace element ratios allow distinguishing plume from

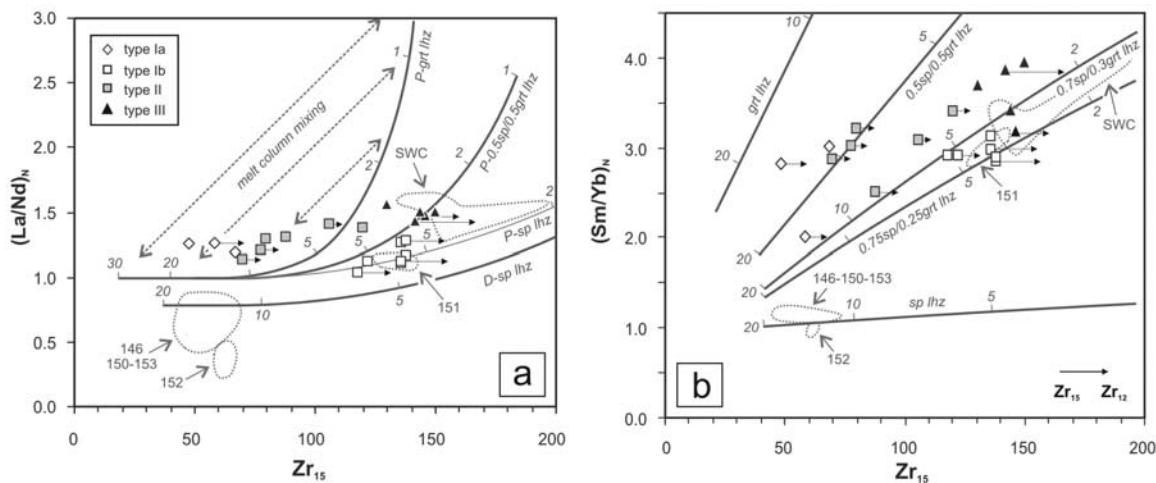


Figure 12. (a) Zr_{15} versus $(La/Nd)_N$ and (b) Zr_{15} versus $(Sm/Yb)_N$ diagrams for the Duarte Complex rocks, and models of pooled fractional melting of various, possible mantle source regions [Kerr *et al.*, 2002] used for petrogenetic interpretation. The mantle sources include depleted mantle (D), more enriched (P, primitive) mantle, garnet lherzolite (gt lhz), 50:50 or 75:25 spinel-garnet lherzolite mixtures, and spinel lherzolite (sp lhz). Numbered ticks on the melting curves indicate percentage of partial melting and Zr_{15} indicates the calculated Zr content for 15 wt % MgO. See text for discussion.

MORB source regions (see below). On the other hand, the HREE depletion that characterizes Duarte Complex rocks suggests that they formed from a mantle source region containing some garnet. The negative correlation between $(\epsilon_{Nd})_i$ and $(Sm/Yb)_N$ displayed by the samples in Figure 11d, reveals that the more enriched melts are derived from deeper source region and vice versa.

[29] To evaluate the depleted or enriched nature of the plume source region that gave rise to the Duarte Complex magmas, selected compositions for each geochemical group were compared with the pooled fractional melting calculations for various possible mantle sources. These sources were modeled by Kerr *et al.* [2002] and range from depleted mantle to more enriched (primitive) mantle, and from garnet lherzolite through a 50:50 spinel-garnet lherzolite mixture to spinel lherzolite. The modeled melt compositions for different percentage of partial melting (i.e., melting at discrete depths within the plume) and different source compositions are plotted in Figure 12. To minimize the effects of fractional crystallization and crystal accumulation, a MgO value of 15 wt % was chosen for each parental magma (high-, mid-, and low-Ti trends) and the theoretical Zr_{15} content of each sample at this MgO value was calculated following the methodology of Kerr *et al.* [2002]. Parental magmas with 15 wt % MgO would have been in equilibrium with Fo₉₀₋₈₆ olivine phenocrysts [Spadea *et al.*, 1989; Révillon *et al.*, 2000].

6.2. Source Characterization of the Duarte Complex Groups

[30] As discussed previously, the Duarte Complex contains compositionally diverse groups derived from different mantle sources as modeled in Figure 12. The source of group Ia magmas ($[La/Nd]_N < 1.0-1.5$; $[Sm/Yb]_N = 1.9-3.0$; $Zr_{15} < 70$) was primitive garnet lherzolite mantle (Figure 12a), that was enriched in incompatible elements, relatively LREE-depleted and a $(\epsilon_{Nd})_i$ value of 6.5, with

respect to MORB source mantle. The genesis of group Ia magmas requires therefore a high melting degree (14–20%) of such a source. As is shown in Figure 12a, the composition of group Ia magmas can be also explained by mixing of melts produced by low melting degree (<2%) of deep garnet lherzolite and higher melting degree (>10%) of a shallower mantle source within a mantle melt column.

[31] The source of group Ib magmas ($[La/Nd]_N < 1.0-1.2$; $[Sm/Yb]_N = 2.8-3.1$; $Zr_{15} = 120-140$) was primitive mantle consisting of spinel lherzolite with, from their position near the 50:50 mixture curve, probably small amounts of garnet lherzolite (Figure 12a). This source was also enriched relative to depleted MORB source mantle, but depleted relative to those of the other magma groups, consistent with LREE depletion patterns and higher $(\epsilon_{Nd})_i > +6.2-6.6$ values. This source underwent about 6–7% melting to form group Ib magmas. Modeling of melting in Figure 12b indicates that group Ib magmas were also generated by about 5% melting of mostly spinel lherzolite source with some amounts of garnet lherzolite. Group Ib rocks are similar to samples from Site 151 of DSDP that drilled the CCOP [Kerr *et al.*, 1996, 1997b].

[32] The source of voluminous group II magma ($[La/Nd]_N = 1.2-1.4$; $[Sm/Yb]_N = 2.4-3.4$; $Zr_{15} < 120$) was enriched mantle consisting of primitive garnet lherzolite, that underwent ~10% melting (Figure 12a), or a mixture of 50:50 garnet and spinel lherzolite that underwent 5–10% melting (Figure 12b). However, the composition of group II picrites could also be explained by the mixing process within the melt column, as discussed above for group Ia magmas. These magmas result by mixing of very small degree melts (~2%) of a deeper garnet lherzolite region and 8–10% melting of a shallower source region. Group II samples are similar to picrites from El Encenillo, SW Colombia, and other enriched CCOP volcanic rocks [Costa Rica and Gorgona, Kerr *et al.*, 1997a, 2002].

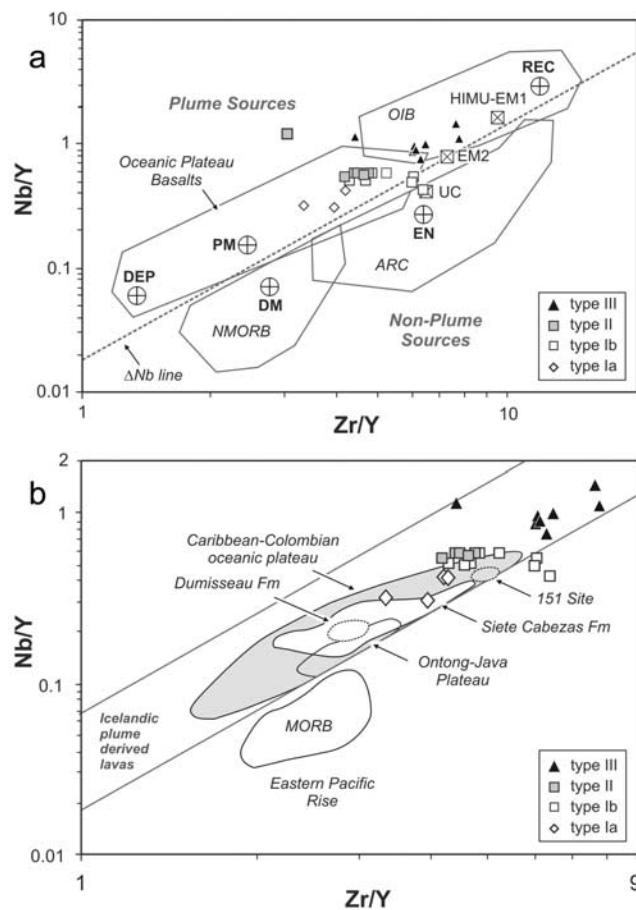


Figure 13. Samples of the Duarte Complex plotted in a log-log diagram of Nb/Y versus Zr/Y after *Fitton et al.* [1997]. (a) End-members of mantle compositional components and the fields of basalts from various tectonic settings taken from *Condie* [2005, and references herein]. Abbreviations: UC, upper continental crust; PM, primitive mantle; DM, shallow depleted mantle; HIMU, high- μ (U/Pb) source; EM1 and EM2, enriched mantle sources; ARC, arc-related basalts; NMORB, normal ocean ridge basalt; OIB, oceanic island basalt; DEP, deep depleted mantle; EN, enriched component; REC, recycled component. (b) Fragments of the CCOP in Hispaniola: Duarte Complex (this work), Dumisseau Formation [*Sen et al.*, 1988], and Siete Cabezas Formation (*J. Escuder-Viruete*, unpublished data, 2006) that plot within the tram lines defined by Icelandic mantle plume lavas. East Pacific Rise MORB lavas [*Mahoney et al.*, 1994] plot below this field. Other data sources are as in Figure 11.

[33] Group III basalts ($[La/Nd]_N = 1.4-2.0$; $[Sm/Yb]_N > 3.0$) are consistent with an enriched mantle source containing garnet, as shown by the highest values in the $[La/Nd]_N$ and $(Sm/Yb)_N$ ratios, and the lowest positive $(\epsilon_{Nd})_i < +5.2$ values in the analyzed sample set. The generation of group III magma can be modeled by about 3–4% melting of 50:50 mixture of primitive garnet and spinel lherzolite (Figure 12a), or 2–3% melting of a 75:25 mixture more spinel lherzolite-rich (Figure 12b). This mantle source was

therefore deeper and underwent a lower degree of melting than the sources of groups I and II.

6.3. Mantle Reservoirs and Implications

[34] Using basalt compositions from the Iceland plume, *Fitton et al.* [1997] suggest that a deep depleted mantle source can be distinguished from the shallow normal MORB (NMORB) source using Zr/Y and Nb/Y ratios. In a log-log Zr/Y versus Nb/Y diagram, the ΔNb line separating plume from nonplume basaltic sources seems to provide good discrimination (Figure 13a), because basalts plotting below the ΔNb line are those derived from either a shallow depleted source (DM), from subduction zones, or from a plume that has been contaminated by continental lithosphere. In the Nb/Y versus Zr/Y diagram (Figure 13a), the Duarte Complex samples are characterized in terms of mantle components and compared with other plume-related igneous units of the CCOP. In this diagram, almost all Duarte Complex picrites and high-Mg basalts plot above the ΔNb line in the mantle plume field, in the oceanic plateau (lower unit) and oceanic island basalt (upper unit) fields of *Condie* [2005]. This is consistent with our previous inference that these rocks derive from a heterogeneous mantle plume source. Moreover, the different Duarte Complex geochemical groups define a linear array that suggests mixing between a deep depleted component (DEP) and a recycled mantle component (REC). From group I and II to group III rocks, the REC component increases but group III rocks plot in the oceanic island basalt field, out of the field of oceanic plateau basalts. In a mantle plume model, these relations suggest high-degree melting of plume heads to generate the lower unit picrites and high-Mg basalts, and a larger contribution from plume tails to generate group III basalts. Some of group Ia and Ib samples have an enriched component (EN), which may be a consequence of contamination by continental crust, as documented for example in the early states of the Kerguelen Plateau [*Weis et al.*, 2001], or interaction with the subcontinental lithosphere. It would appear that the earlier stages of the evolution of the Duarte Complex plume might have involved interaction with the continental lithosphere below North or South America, linked previously to the breakup of Pangea. Alternatively, this enriched component in the magma sources of some samples may represent recycled continental sediments.

6.4. Significance of Lower Cretaceous Plume Volcanism in Hispaniola

[35] *Kerr et al.* [1997a] have shown that oceanic plateau basalts from the Caribbean-Colombian and Ontong Java oceanic plateaus plot between two “tramlines” defined in the log Nb/Y – log Zr/Y diagram by the plume-derived lavas from Iceland. Similarities between Icelandic and Caribbean lavas have suggested to *Kerr et al.* [1997a] that CCOP formed at, or near, an oceanic spreading center. The geochemical similarity of the Duarte Complex samples and other plume-derived units present in Hispaniola provide some constraints in this respect: (1) if all rocks derived from the same mantle plume and (2) if the plume had a prolonged, unique history of activity.

[36] With respect to the first question, i.e., a common mantle plume source for CCOP lavas, the geochemical diversity of the Duarte Complex array shown in Figure 13b

does not indicate a depleted MORB mantle source region, although these lavas, in particular, groups Ia and Ib, are depleted relative to bulk earth with positive (ϵ_{Nd})_i > +5 values. A shallow depleted mantle source is represented in Figure 13b by the East Pacific Rise MORB field [Mahoney *et al.*, 1994], which plots below the ΔNb line. Figure 13b shows the elongated field of the Late Cretaceous (91–88 Ma) CCOP igneous rocks, including the basalts drilled during DSDP Leg 15 in the Caribbean seafloor [Sinton *et al.*, 1998; Hauff *et al.*, 2000a; Kerr *et al.*, 2002] and those from Dumisseau Formation in Haiti [Sen *et al.*, 1988]. The DSDP Site 151 samples exhibit high contents of incompatible trace elements, close to those of the Duarte Complex group Ib and II samples. Only group Ia samples are similar to the more enriched CCOP lavas, and most of the CCOP field is more depleted, including the Dumisseau Formation and Ontong Java oceanic plateau lavas. The middle Campanian to Maastrichtian Siete Cabezas Formation basalts from central Hispaniola have been related to the CCOP [Sinton *et al.*, 1998]. This is consistent with their plot in Figure 13b, within the same field of the CCOP lavas, that suggests a mantle plume source, as previously supposed by Lewis *et al.* [2002]. However, the Siete Cabezas Formation lavas are in terms of incompatible trace elements ratios distinct from those of the Duarte Complex, particularly from the group III basalts of the upper unit. Therefore, if the plume responsible of the CCOP had a long history of activity, the primary mantle melts were generated within different and heterogeneous source regions during the Early and Late Cretaceous.

[37] With respect to the second question, i.e., a prolonged history of CCOP-related plume, the stratigraphic geochemical and geochronological data of the Duarte Complex demonstrate than an Early Cretaceous phase of CCOP construction onto Late Jurassic proto-Caribbean oceanic crust is recorded in the Cordillera Central of Hispaniola. The wide compositional range that the Duarte Complex displays was derived from the same mantle plume through time, which had a marked heterogeneity. Therefore more than one Cretaceous oceanic plateau is preserved in Hispaniola as suggested by Sinton *et al.* [1998] and Lewis *et al.* [2002]. Alternatively, several pulses of magmatism separated by protracted periods at a much lower rate linked to the same plume were recorded, as in other localities of the Caribbean plate [Lapierre *et al.*, 2002] and in the eastern Pacific oceanic plateaus [Ernst *et al.*, 2005].

7. Conclusions

[38] The Duarte Complex from the western Cordillera Central of Hispaniola comprises a thick sequence of picrites, high-Mg basalts and basalts, as well as metamorphic equivalents. Geochemical data show that the complex includes four geochemical groups, which make up two lithostratigraphic units. TiO₂ contents, Sr-Nd isotope and incompatible trace element systematics are consistent with mantle sources related to a heterogeneous plume. These data and mantle melt modeling suggests that plume mantle sources of magmas were more enriched and deeper through time. Although all Duarte Complex rocks show evidence of a long-time depleted source region ($[\epsilon_{Nd}]_i > +5$), REE contents, Sr-Nd isotopic ratios and Nb/Y versus Zr/Y

systematics reveal that this source region is not a depleted, NMORB source, mantle, but a depleted source region intrinsic to the plume. Incompatible trace element ratios suggest a mixing between this depleted component and recycled mantle component, which is some combination of HIMU and EM1 - EM2 end-members (i.e., recycled oceanic crust and pelagic sediments). The ⁴⁰Ar-³⁹Ar plateau ages of synkinematic hornblende in foliated amphibolites of the Duarte Complex are Cenomanian, and indicate a >96 Ma older age of the CCOP volcanic protoliths.

[39] **Acknowledgments.** The authors thank John Lewis (George Washington University) and Gren Draper (Florida International University) for their introduction to the area, initial fieldwork, and continued discussions and advice on the petrology and geochemistry of volcanic rocks in the Dominican Republic. Elisa Dietrich-Sainsaulieu is thanked for her help with the Sr-Nd isotopic analyses of the samples at PCIGR. This work forms part of the geothematic cartographic project of the Dominican Republic funded by the SYSMIN Project of the EU and received financial aid from MCYT projects BTE-2002-00326 and CGL2005-02162/BTE. We wish to thank Dirección General de Minería for support in Dominican Republic. Constructive reviews from John Lewis, Andrew Kerr, and Robert Duncan are much appreciated, as was the editorial assistance of Richard Arculus.

References

- Alvarado, G. E., P. Denyer, and C. W. Sinton (1997), The 89 Ma Tortugal komatiitic suite, Costa Rica: Implications for a common geological origin of the Caribbean and eastern Pacific region from a mantle plume, *Geology*, **25**, 439–442.
- Arndt, N. T. (1999), Why was flood volcanism on submerged continental platforms so common in the Precambrian?, *Precambrian Res.*, **97**, 155–164.
- Arndt, N. T., A. C. Kerr, and J. Tarney (1997), Dynamic melting in plume heads: The formation of Gorgona komatiites and basalts, *Earth Planet. Sci. Lett.*, **146**, 289–301.
- Bédart, J. H. (1999), Petrogenesis of boninites from the Betts Cove Ophiolite, Newfoundland, Canada: Identification of subducted source components, *J. Petrol.*, **40**, 1853–1889.
- Bienvenu, P., H. Bougault, J. L. Joron, M. Treuil, and L. Demitriev (1990), REE/non REE element hygromagmaphile element fractionation, *Chem. Geol.*, **82**, 1–14.
- Boudreau, A. E. (1999), PELE: A version of the MELTS software program for the PC platform, *Comput. Geosci.*, **25**, 20–201.
- Campbell, I. H., R. W. Griffiths, and R. I. Hill (1989), Melting in an Archean mantle plume: Heads its basalts, tails its komatiites, *Nature*, **339**, 697–699.
- Coffin, M. F., and O. Eldholm (1994), Large igneous provinces: Crustal structure, dimensions, and external consequences, *Rev. Geophys.*, **32**, 1–36.
- Condie, K. C. (2005), High field strength element ratios in Archean basalts: A window to evolving sources of mantle plumes?, *Lithos*, **79**, 491–504.
- Contreras, F., et al. (2004), Mapa geológico de la República Dominicana escala 1:50,000, Monción, 210 pp., Dir. Gen. de Minería, Santo Domingo.
- de Lepinay, B. M. (1987), L'évolution géologique de la bordure Nord-Caraïbe: L'exemple de la transversale de l'île d'Española (Grandes Antilles), Ph. D. thesis, 378 pp., Univ. Pierre et Marie Curie, Paris.
- Donnelly, T. W., et al. (1990), History and tectonic setting of Caribbean magmatism, in *The Geology of North America*, vol. H, *The Caribbean Region*, edited by G. Dengo and J. E. Case, pp. 339–374, Geol. Soc. of Am., Boulder, Colo.
- Draper, G., and J. F. Lewis (1989), Petrology and structural development of the Duarte complex, central Republica Dominicana: A preliminary account and some tectonic implications, in *Transactions of the 10th Caribbean Geological Conference*, edited by H. Duque Caro, pp.103–112, INGEOMINAS, Bogota, Colombia.
- Draper, G., and J. F. Lewis (1991), Metamorphic belts in central Española, in *Geologic and Tectonic Development of the North America-Caribbean Plate Boundary in Española*, edited by P. Mann, G. Draper, and J. Lewis, *Spec. Pap. Geol. Soc. Am.*, **262**, 29–46.
- Duncan, R. A., and R. B. Hargreaves (1984), Plate tectonic evolution of the Caribbean region in the mantle reference frame, in *The Caribbean-South American Plate Boundary and Regional Tectonics*, edited by W. E. Bonini, R. B. Hargreaves, and R. Shagam, *Mem. Geol. Soc. Am.*, **162**, 81–94.
- Dupré, B., and L. M. Echeverría (1984), Pb isotopes of Gorgona island (Colombia): Isotopic variations correlated with magma type, *Earth Planet. Sci. Lett.*, **67**, 186–190.

- Ernst, R. E., K. L. Buchan, and I. H. Campbell (2005), Frontiers in large igneous province research, *Lithos*, 79, 271–297.
- Escuder-Virueite, J., F. Contreras, G. Stein, P. Urien, M. Joubert, E. Bernardez, P. P. Hernández Huerta, J. Lewis, E. Lopera, and A. Pérez-Estaún (2004), La secuencia magmática Jurásico Superior-Cretácico Superior en la Cordillera Central, República Dominicana: Sección cortical de un arco-isla intraoceánico, *Geo-Temas*, 6, 41–44.
- Escuder-Virueite, J., F. Contreras, G. Stein, P. Urien, M. Joubert, T. D. Ullrich, J. Mortensen, and A. Pérez-Estaún (2006), Transpression and strike-slip partitioning in the Caribbean island arc: Fabric development, kinematics and Ar-Ar ages of syntectonic emplacement of the Loma de Cabrera batholith, Dominican Republic, *J. Struct. Geol.*, 28, 1496–1519.
- Fitton, J. G., A. D. Saunders, M. J. Norry, B. S. Hardarson, and R. N. Taylor (1997), Thermal and chemical structure of the Iceland plume, *Earth Planet. Sci. Lett.*, 153, 197–208.
- Fitton, J. G., A. D. Saunders, P. D. Kempton, and B. S. Hardarson (2003), Does depleted mantle form an intrinsic part of the Iceland plume?, *Geochim. Geophys. Geosyst.*, 4(3), 1032, doi:10.1029/2002GC000424.
- Frey, F. A., K. Nicolaysen, B. K. Kubit, D. Weis, and A. Giret (2002), Flood basalts from Mont Tourmente in the Central Kerguelen Archipelago: The change from tholeiitic/transitional to alkalic basalts at ~25 Ma, *J. Petrol.*, 43, 1367–1387.
- Frey, F. A., M. F. Coffin, P. Wallace, and D. Weis (2003), Leg 183 synthesis: Kerguelen Plateau—Broken Ridge—A large igneous province, *Proc. Ocean Drill. Program Sci. Results* [CD-ROM], 183, 48 pp.
- Gradstein, F. M., J. G. Ogg, and A. G. Smith (2004), *A Geologic Time Scale 2004*, 610 pp., Cambridge Univ. Press, New York.
- Hauff, F., K. Hoernle, G. Tilton, D. W. Graham, and A. C. Kerr (2000a), Large volume recycling of oceanic lithosphere over short time scales: Geochemical constraints from the Caribbean large igneous province, *Earth Planet. Sci. Lett.*, 174, 247–263.
- Hauff, F., K. Hoernle, P. van den Bogaard, G. Alvarado, and D. Garbe-Schönberg (2000b), Age and geochemistry of basaltic complexes in western Costa Rica: Contributions to the geotectonic evolution of Central America, *Geochim. Geophys. Geosyst.*, 1(5), doi:10.1029/1999GC000020.
- Herzberg, C., and M. J. O'Hara (2002), Plume-associated ultramafic magmas of Phanerozoic age, *J. Petrol.*, 43, 1857–1883.
- Hoernle, K., F. Hauff, and P. van den Bogaard (2004), 70 m.y. history (139–69 Ma) for the Caribbean large igneous province, *Geology*, 32, 697–700.
- Jensen, L. S. (1976), A new cation plot for classifying subalkalic volcanic rocks, *Misc. Pap.* 66, Ont. Dep. of Mines, Ottawa, Canada.
- Joubert, M., et al. (2004), Mapa geológico de la República Dominicana a E. 1:50,000, Lamedero, 192 pp., Dir. G. Miner., Santo Domingo.
- Kerr, A. C. (2005), La Isla de Gorgona, Colombia: A petrological enigma?, *Lithos*, 84, 77–101.
- Kerr, A. C., and J. Tarney (2005), Tectonic evolution of the Caribbean and northwestern South America: The case for accretion of two Late Cretaceous oceanic plateaus, *Geology*, 33, 269–272.
- Kerr, A. C., A. D. Saunders, J. Tarney, N. H. Berry, and V. L. Hards (1995), Depleted mantle plume geochemical signatures: No paradox for plume theories, *Geology*, 23, 843–846.
- Kerr, A. C., G. F. Marriner, N. T. Arndt, J. Tarney, A. Nivia, A. D. Saunders, and R. A. Duncan (1996), The petrogenesis of Gorgona komatiites, picrites and basalts: New field, petrographic and geochemical constraints, *Lithos*, 37, 245–260.
- Kerr, A. C., G. F. Marriner, J. Tarney, A. Nivia, A. D. Saunders, M. F. Thirlwall, and C. W. Sinton (1997a), Cretaceous basaltic terranes in western Colombia: Elemental, chronological and Sr-Nd constraints on petrogenesis, *J. Petrol.*, 38, 677–702.
- Kerr, A. C., J. Tarney, G. F. Marriner, A. Nivia, and A. D. Saunders (1997b), The Caribbean-Colombian Cretaceous igneous province: The internal anatomy of an oceanic plateau, in *Large Igneous Provinces: Continental, Oceanic, and Planetary Flood Volcanism*, *Geophys. Monogr. Ser.*, vol. 100, edited by J. J. Mahoney and M. F. Coffin, pp. 123–144, AGU, Washington, D. C.
- Kerr, A. C., J. Tarney, P. D. Kempton, P. Spadea, A. Nivia, G. F. Marriner, and R. A. Duncan (2002), Pervasive mantle plume head heterogeneity: Evidence from the late Cretaceous Caribbean-Colombian oceanic plateau, *J. Geophys. Res.*, 107(B7), 2140, doi:10.1029/2001JB000790.
- Lapierre, H., V. Dupuis, B. M. de Lepinay, M. Tardy, J. Ruiz, R. C. Maury, J. Hernández, and M. Loubet (1997), Is the Lower Duarte Complex (Española) a remnant of the Caribbean plume generated oceanic plateau?, *J. Geol.*, 105, 111–120.
- Lapierre, H., et al. (1999), Late Jurassic oceanic crust and upper Cretaceous Caribbean plateau picritic basalts exposed in the Duarte igneous complex, Hispaniola, *J. Geology*, 107, 193–207.
- Lapierre, H., et al. (2000), Multiple plume events in the genesis of the peri-Caribbean Cretaceous oceanic plateau province, *J. Geophys. Res.*, 105, 8403–8421.
- Lewis, J. F., and J. G. Jiménez (1991), Duarte Complex in the La Vega-Jarabacoa-Jánico Area, central Española: Geological and geochemical features of the sea floor during the early stages of arc evolution, in *Geologic and Tectonic Development of the North America-Caribbean Plate Boundary in Hispaniola*, edited by P. Mann, G. Draper, and J. F. Lewis, *Spec. Pap. Geol. Soc. Am.*, 262, 115–142.
- Lewis, J. F., G. Draper, and D. Burgi (1983), Geochemistry and petrology of high magnesian metabasalts of the Duarte Complex, Dominican Republic, in *Transactions of the 10th Caribbean Geological Conference*, edited by H. Duque Caro, pp. 47–48, INGEOMINAS, Bogota, Colombia.
- Lewis, J. F., W. E. Hames, and G. Draper (1999), Late Jurassic oceanic crust and Upper Cretaceous Caribbean Plateau picritic basalts exposed in the Duarte igneous complex, Española: A discussion, *J. Geol.*, 107, 505–508.
- Lewis, J. F., J. Escuder-Virueite, P. P. Hernaiz Huerta, G. Gutiérrez, G. Draper, and A. Pérez-Estaún (2002), Subdivisión geoquímica del Arco Isla Circum-Caribeño, Cordillera Central Dominicana: Implicaciones para la formación, acreción y crecimiento cortical en un ambiente intraoceánico, *Acta Geol. Hisp.*, 37, 81–122.
- Mahoney, J. J., J. M. Sinton, J. D. MacDougall, K. J. Spencer, and G. W. Lugmair (1994), Isotope and trace element characteristics of a super-fast spreading ridge: East Pacific Rise, 13–238S, *Earth Planet. Sci. Lett.*, 121, 173–193.
- Mann, P. (1999), Caribbean sedimentary basins: Classification and tectonic setting from Jurassic to Present, in *Sedimentary Basins of the World*, vol. 4, *Caribbean Basins*, edited by P. Mann, pp. 3–31, Elsevier, New York.
- McDonough, W. F., and T. R. Ireland (1993), Intra-plate origin of komatiites inferred from trace element in glass inclusions, *Nature*, 365, 432–434.
- Meschede, M. (1998), The impossible Galapagos connection: Geometric constraints for a near-American origin of the Caribbean plate, *Geol. Rundsch.*, 87, 200–205.
- Montgomery, H., and E. A. Pessagno (1999), Cretaceous microfaunas of the Blue mountains, Jamaica, and of the northern and central basement complexes of Hispaniola, Caribbean, in *Sedimentary Basins of the World*, vol. 4, *Caribbean Basins*, edited by P. Mann, pp. 237–246, Elsevier, New York.
- Montgomery, H., E. A. Pessagno, J. F. Lewis, and J. Schellekens (1994), Paleogeography of Jurassic fragments in the Caribbean, *Tectonics*, 13, 725–732.
- Neal, C. R., J. J. Mahoney, L. W. Kroenke, R. A. Duncan, and M. G. Pettersen (1997), The Ontong Java Plateau, in *Continental, Oceanic, and Planetary Flood Volcanism*, *Geophys. Monogr. Ser.*, vol. 100, edited by J. J. Mahoney and M. F. Coffin, pp. 183–216, AGU, Washington, D. C.
- Palmer, H. C. (1979), Geology of the Monción-Jarabacoa area, Dominican Republic, in *Tectonic Focal Point of the North Caribbean*, edited by B. Lidz and F. Nagle, pp. 29–68, Miami Geol. Soc., Miami, Fla.
- Pilidou, S., K. Priestley, E. Debayle, and O. Gudmundsson (2005), Rayleigh wave tomography in the North Atlantic: High resolution images of the Iceland, Azores and Eifel mantle plumes, *Lithos*, 79, 453–474.
- Pindell, J. L., L. Kennan, W. V. Maresch, K. P. Stanek, G. Draper, and R. Higgs (2005), Plate-kinematics and crustal dynamics of circum-Caribbean arc-continent interactions: Tectonic controls on basin development in Proto-Caribbean margins, in *Caribbean-South American Plate Interactions*, edited by A. Lallemand and V. B. Sisson, *Spec. Pap. Geol. Soc. Am.*, 394, 7–52.
- Pindell, J. L., L. Kennan, K. P. Stanek, W. V. Maresch, and G. Draper (2006), Foundations of Gulf of Mexico and Caribbean evolution: Eight controversies resolved, *Geol. Acta*, 4, 303–341.
- Révillon, S., N. T. Arndt, C. Chauvel, and E. Hallot (2000), Geochemical study of ultramafic volcanic and plutonic rocks from Gorgona island, Colombia: The plumbing system of an oceanic plateau, *J. Petrol.*, 41, 1127–1153.
- Révillon, S., C. Chauvel, N. T. Arndt, R. Pik, F. Martineau, S. Fourcade, and B. Marty (2002), Heterogeneity of the Caribbean plateau mantle source: Sr, O and He isotopic compositions of olivine and clinopyroxene from Gorgona island, *Earth Planet. Sci. Lett.*, 205, 91–106.
- Saunders, A. D., J. Tarney, A. C. Kerr, and R. W. Kent (1996), The formation and fate of large oceanic igneous provinces, *Lithos*, 37, 81–95.
- Sen, G., D. G. Hickey-Vargas, F. Waggoner, and F. Maurasse (1988), Geochemistry of basalts from the Dumisseau Formation, southern Haiti: Implications for the origin of the Caribbean Sea crust, *Earth Planet. Sci. Lett.*, 87, 423–437.
- Sinton, C. W., R. A. Duncan, M. Storey, J. Lewis, and J. J. Estrada (1998), An oceanic flood basalt province within the Caribbean plate, *Earth Planet. Sci. Lett.*, 155, 221–235.
- Sinton, C. W., H. Sigurdsson, and R. A. Duncan (2000), Geochronology and petrology of the igneous basement at the Lower Nicaraguan Rise, Site 1001, *Proc. Ocean Drill. Program Sci. Results*, 165, 233–236.

- Spadea, P., E. Espinosa, and A. Orrego (1989), High-MgO extrusive rocks from the Romeral Zone ophiolites in the southwestern Colombian Andes, *Chem. Geol.*, *77*, 32–303.
- Sun, S. S., and W. F. McDonough (1989), Chemical and isotopic systematics of oceanic basalts: Implications for mantle compositions and processes, in *Magmatism in the Ocean Basins*, edited by A. D. Saunders and M. J. Norry, *Geol. Soc. Spec. Publ.*, *42*, 313–345.
- Swinden, H. S., G. A. Jenner, B. J. Fryer, J. Hertogen, and J. C. Roddick (1990), Petrogenesis and paleotectonic history of the Wild Bight Group, an Ordovician rifted island arc in central Newfoundland, *Contrib. Mineral. Petrol.*, *105*, 219–241.
- Weis, D., and F. A. Frey (2002), Submarine basalts of the northern Kerguelen Plateau: Interaction between the Kerguelen Plume and the Southeast Indian Ridge revealed at ODP Site 1140, *J. Petrol.*, *43*, 1287–1309.
- Weis, D., S. Ingle, D. Damasceno, F. A. Frey, K. Nicolaysen, J. Barling, and Leg 183 Shipboard Scientific Party (2001), Origin of continental components in Indian Ocean basalts: Evidence from Elan Bank (Kerguelen Plateau, ODP Leg 183, Site 1137), *Geology*, *29*, 147–150.
-
- F. Contreras, INYPSA, C. General Díaz Porlier 49, E-28001 Madrid, Spain. (fcontrerasvazquez@gmail.com)
- J. Escuder-Virueite, Instituto Geológico y Minero de España, C. Ríos Rosas 23, E-28003 Madrid, Spain. (j.escuder@igme.es)
- M. Joubert, BRGM, Av. C. Guillemin, F-45060 Orléans, France. (m.joubert@brgm.fr)
- A. Pérez-Estaún, ICT Jaume Almera, CSIC, Lluís Solé i Sabarís s/n, E-08028 Barcelona, Spain. (andres@ija.csic.es)
- T. D. Ullrich and D. Weis, Pacific Centre for Isotopic and Geochemical Research, University of British Columbia, 6339 Stores Road Vancouver, BC, Canada V6T 1Z4. (tullrich@eos.ubc.ca; dweis@eos.ubc.ca)